HHS Public Access

Author manuscript

Cell. Author manuscript; available in PMC 2021 July 23.

Published in final edited form as:

Cell. 2020 July 23; 182(2): 447–462.e14. doi:10.1016/j.cell.2020.05.048.

The Intermucosal Connection between the Mouth and Gut in Commensal Pathobiont-Driven Colitis

Sho Kitamoto[1], **Hiroko Nagao-Kitamoto**[1], **Yizu Jiao**[2,5], **Merritt G. Gillilland III**[1], **Atsushi Hayashi**[1,6], **Jin Imai**[1], **Kohei Sugihara**[1], **Mao Miyoshi**[1], **Jennifer C. Brazil**[2], **Peter Kuffa**[1], **Brett D. Hill**[4], **Syed M. Rizvi**[4], **Fei Wen**[4], **Shrinivas Bishu**[1], **Naohiro Inohara**[2], **Kathryn A. Eaton**[3], **Asma Nusrat**[2], **Yu L. Lei**[4], **William V. Giannobile**[5], **Nobuhiko Kamada**[1,7,*]

[1]Division of Gastroenterology and Hepatology, Department of Internal Medicine, University of Michigan, Ann Arbor, MI, USA

[2]Department of Pathology, University of Michigan, Ann Arbor, MI, USA

[3]Department of Microbiology and Immunology, University of Michigan, Ann Arbor, MI, USA

[4]Department of Chemical Engineering, University of Michigan, Ann Arbor, MI, USA

[5]Department of Periodontics and Oral Medicine, University of Michigan School of Dentistry, Ann Arbor, MI, USA

[6]Research Laboratory, Miyarisan Pharmaceutical Co., Ltd., Tokyo, Japan

[7]Lead Contact

SUMMARY

The precise mechanism by which oral infection contributes to the pathogenesis of extra-oral diseases remains unclear. Here, we report that periodontal inflammation exacerbates gut inflammation *in vivo*. Periodontitis leads to expansion of oral pathobionts, including *Klebsiella* and *Enterobacter* species, in the oral cavity. Amassed oral pathobionts are ingested and translocate to the gut, where they activate the inflammasome in colonic mononuclear phagocytes, triggering inflammation. In parallel, periodontitis results in generation of oral pathobiont-reactive Th17 cells in the oral cavity. Oral pathobiont-reactive Th17 cells are imprinted with gut tropism and migrate to the inflamed gut. When in the gut, Th17 cells of oral origin can be activated by translocated oral pathobionts and cause development of colitis, but they are not activated by gut-resident microbes. Thus, oral inflammation, such as periodontitis, exacerbates gut inflammation by supplying the gut with both colitogenic pathobionts and pathogenic T cells.

[*]Correspondence: nkamada@umich.edu.

AUTHOR CONTRIBUTIONS

S.K. and N.K. conceived and designed the experiments. S.K. conducted most of the experiments with help from H.N.-K., A.H., M.M., J.I., K.S., P.K., and S.B. M.G.G. performed microbiome analysis. Y.J., N.I., and W.V.G. contributed to the establishment of the murine periodontitis model. J.C.B. and A.N. contributed to the establishment of the two-dimensional colonoid model. K.A.E. helped with GF animal experiments. B.D.H. and F.W. contributed the establishment of the CyTOF antibody panel. S.M.R. and Y.L.L. conducted the CyTOF analysis. S.K. and N.K. analyzed the data. S.K. and N.K. wrote the manuscript with contributions from all authors.

DECLARATION OF INTERESTS

The authors declare no competing interests.

SUPPLEMENTAL INFORMATION

Supplemental Information can be found online at https://doi.org/10.1016/j.cell.2020.05.048.

In Brief

Periodontitis leads to expansion of pathobiont members of the oral microbiota, which promote colitis via colonization of the gut as well as induction of migratory Th17 cells, constituting a dual microbiome and immune mechanism linking oral and gut health.

Graphical Abstract

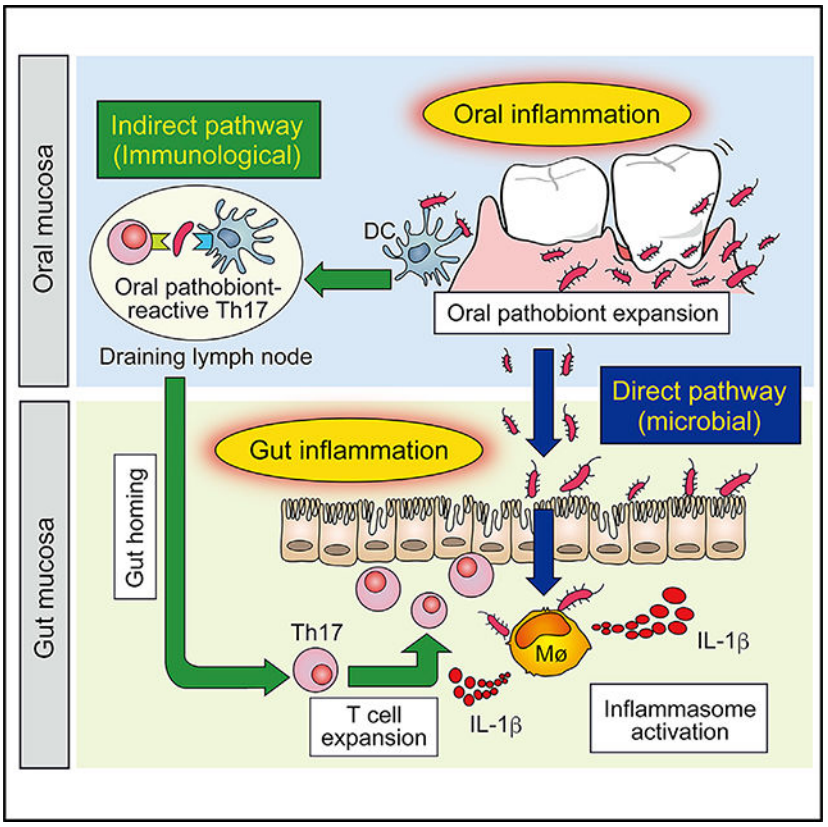

INTRODUCTION

Recent accumulating evidence suggests a possible “mouth-gut axis” in the context of pathogenesis of gastrointestinal diseases, such as inflammatory bowel disease (IBD) as well as colorectal cancer (Garrett, 2015; Irrazábal et al., 2014; Said et al., 2014). The oral cavity is a common site of extra-intestinal manifestations of IBD, especially Crohn’s disease (CD) (Brandtzaeg, 2001; Brito et al., 2008; Lankarani et al., 2013; Lourenço et al., 2010; Van Dyke et al., 1986; Vavricka et al., 2013). The prevalence of periodontitis is significantly increased in CD patients compared with non-IBD control individuals (Brandtzaeg, 2001; Brito et al., 2008; Van Dyke et al., 1986; Vavricka et al., 2013). Likewise, SAMP1/YitFc mice, a murine model of CS, concurrently develop periodontal inflammation, and the severity of periodontitis correlates with that of ileitis (Pietropaoli et al., 2014). These observations suggest the possibility that the inflammatory processes occurring at oral and gut mucosae are somehow connected. However, the extent to which periodontal inflammation influences gastrointestinal diseases remains to be fully elucidated.

It has become evident that typical mouth-resident bacteria, such as Fusobacteriaceae, Pasteurellaceae, and Veillonellaceae, are enriched in the mucosal tissues of IBD patients (Gevers et al., 2014; Haberman et al., 2014; Schirmer et al., 2018). Likewise, *Klebsiella* species, isolated from the saliva of IBD patients, have been identified as pathobionts whose ectopic colonization in the intestine elicits development of colitis (Atarashi et al., 2017). Given that the oral mucosa and colonic mucosa are physically connected, ingested oral bacteria likely translocate to the lower digestive tract, where they can elicit pathogenic immune responses. In addition to accumulation of pathobionts, bacteria-reactive $CD4^+$ T cells accumulate in the intestinal mucosa of IBD patients and are believed to play a central role in disease pathogenesis (Calderón-Gómez et al., 2016; Shen et al., 2008). However, the mechanism by which these bacterium-reactive pathogenic T cells arise remains largely unknown. In this regard, it has been reported that the immune cells found in the oral draining lymph nodes can transmigrate to other lymphoid organs, including the gut (Morton et al., 2014). Thus, it is possible that oral inflammation gives rise to the emergence of oral pathobiont-reactive T cells. Pathogenic T cells then transmigrate from the oral mucosa to the gut, where they are activated by gut bacteria and cause intestinal inflammation.

Here we found that periodontitis aggravates gut inflammation in mice. Periodontitis induces expansion of *Klebsiella*/*Enterobacter* species in the oral mucosa. The amassed oral *Klebsiella/Enterobacter* species can translocate to the lower digestive tract and ectopically colonize it. Ectopic colonization of oral *Klebsiella/Enterobacter* species elicits activation of the inflammasome in *lamina propria* macrophages, which may compound their colitogenic capacities. In parallel, oral bacterium-reactive Th17-skewed T cells arise *de novo* in the oral cavity during periodontitis. Oral bacterium-reactive T cells are imprinted with gut tropism and migrate to the inflamed gut. When in the gut, the oral bacterium-reactive T cells are subsequently activated by ectopically colonized oral pathobionts and contribute to gut inflammation. Thus, together, oral pathobionts and pathogenic T cells, generated as a result of oral inflammation, exacerbate gut inflammation.

RESULTS

Periodontitis Aggravates Intestinal Inflammation

To investigate the effect of oral inflammation on gastrointestinal disease, we utilized a ligature-induced periodontitis model (Abe and Hajishengallis, 2013; Jiao et al., 2013). Oral ligature placement resulted in massive alveolar bone loss 14 days post-insertion (Figure S1A). Oral ligation resulted in a transient spike of serum amyloid A (SAA), a non-specific marker of inflammation, 3 and 7 days post-placement, but systemic inflammation had resolved by day 14 (Figure S1B). No translocation of bacteria to the peripheral blood was observed (Figure S1C). In contrast, oral dysbiosis caused by oral ligation persisted (Figure S1D). On day 14 after oral ligation, mice were treated with dextran sodium sulfate (DSS) to induce experimental colitis (Figure 1A). Mice in the ligature-DSS group experienced significantly increased body weight loss and had higher disease activity index (DAI) values (Murthy et al., 1993) compared with the controls (Figures 1B and 1C). Likewise, mice in the ligature-DSS group displayed a greater degree of inflammation in the colonic mucosa compared with the controls (Figures 1D–1F). To further characterize the immune responses

in ligature-DSS mice, we performed a comprehensive CyTOF panel for murine immune profiling (Figure 1G). We performed an unbiased viSNE analysis to reduce the dimensionality of data (Amir et al., 2013). We clustered immune subsets based on surface marker expression profiles and found that DSS treatment dramatically increased myeloid and lymphoid infiltration, as expected (Figure S2). Interestingly, oral ligature treatment alone also enhanced immune infiltration into the gut *lamina propria*, including Th17 subsets, B cells, and γδ T cells (Figure S2; Table S1). Notably, we observed a clear additive effect on expansion of resting and activated Th17 subsets (populations 12 and 14, respectively) in the group that received oral ligature and DSS treatment (Figures 1G and 1H; Figure S2; Table S1). To quantitatively validate the elevated numbers of Th17 cells, we conducted a conventional flow cytometry analysis. Consistent with the results of the CyTOF analysis, $CD3^+CD4^+$ T cells were significantly increased in the ligature-DSS group compared with controls (Figures 1I and 1J). Further characterization demonstrated that $ROR\gamma t^+T\text{-}bet^{+/-}$ Th17 cells and $ROR\gamma t^-T\text{-}bet^+$ Th1 cells were significantly enriched in mice with ligature-DSS compared with DSS alone, whereas the abundance of $Foxp3^+$ Tregs was unchanged (Figures 1K and 1L). Consistently, colonic $CD3^+CD4^+$ T cells isolated from ligature-DSS mice produced significantly more interleukin-17A (IL-17A) and interferon γ (IFN-γ), but not IL-10, than cells isolated from DSS-only or non-colitic control mice (Figure 1M). These results indicate that ligature-induced periodontitis exacerbates gut inflammation with accumulation of Th17 and Th1 cells.

Enterobacteriaceae Accumulate in Both the Oral Cavity and the Gut as a Result of Periodontitis

Next we analyzed the oral and gut microbiomes in ligature-DSS mice. As reported previously, periodontitis resulted in oral dysbiosis (Figure 2A; Figure S1D). Enterobacteriaceae in particular dominated during periodontitis (Figure 2A; Figures S1D and S1F). To identify bacterial taxa that are commonly found in the oral and gut mucosa in the presence of periodontitis, we performed LEfSe analysis (Figure 2B). Interestingly, Enterobacteriaceae (OTU001), the most abundant bacterial taxon in the oral cavity during periodontitis, are also enriched in the gut of ligature-DSS-treated mice compared with DSS-treated mice without ligatures (Figure 2B). We further identified the species of Enterobacteriaceae that commonly colonize the oral and gut mucosae. We found that *Klebsiella* spp. and *Enterobacter* spp. were the most dominant species in the inflamed oral cavity (Figures 2C and 2D). Of note, gut colonization by these bacterial species was increased in mice with ligatures (Figure 2E). These findings suggest that pathobiont blooms in the oral cavity lead to accumulation of the same bacterial species in the gut. Notably, ligature insertion did not lead to gut colonization by these bacterial species in mice without DSS colitis (Figure 2E). This result indicates that the healthy gut microbiota prevents ectopic gut colonization by ingested oral pathobionts. Gut inflammation likely disrupts colonization resistance mediated by the resident gut microbiota, making it possible for oral pathobionts to colonize the gut.

Oral Enterobacteriaceae Colonization Leads to Colitis in Genetically Susceptible Hosts

To validate whether oral pathobionts can elicit pathogenic responses in the gut, oral microbiotas were isolated from healthy (healthy oral microbiota [HOM]) or periodontitis

mice (ligature-associated oral microbiota [LOM]) and reconstituted in germ-free (GF) *Il10*$^{-/-}$ mice. Over the course of the experiment, LOM-colonized *Il10*$^{-/-}$ mice showed impaired body weight gain and increased fecal lipocalin−2 (Lcn2) levels compared with HOM-colonized *Il10*$^{-/-}$ mice (Figures 3A and 3B). Likewise, colonic inflammation was significantly exacerbated in the LOM group compared with the HOM group (Figures 3C–3E). Next, to identify the oral pathobiont strains responsible for induction of colitis, we generated synthetic microbial communities comprised of bacterial strains that represent HOM and LOM, respectively. In the HOM community, several strains belonging to the most abundant genera, *Streptococcus* and *Staphylococcus* (i.e., *Streptococcus salivarius*, *Streptococcus* sp. JS71, and *Staphylococcus xylosus*), were isolated and then mixed to make synthetic HOM (sHOM). To make synthetic LOM (sLOM), several isolated Enterobacteriaceae strains (i.e., *Klebsiella aerogenes*, *K. pneumoniae*, *K. variicola*, *Enterobacter cloacae*, and *E. hormaechei*; Figure 2C), which are most prevalent in the LOM community, were mixed (Figure 3F). These synthetic bacterial communities, which mimic HOM and LOM, were used to colonize GF *Il10*$^{-/-}$ mice. In GF *Il10*$^{-/-}$ mice, sHOM and sLOM colonized equally (Figure 3G). As observed with HOM/LOM colonization, increased levels of fecal Lcn2 and exacerbated pathology were observed in sLOM-colonized *Il10*$^{-/-}$ mice compared with sHOM-colonized *Il10*$^{-/-}$ mice (Figures 3H–3J). Similarly, accumulation of Th17 and Th1 cells increased in sLOM-colonized *Il10*$^{-/-}$ mice compared with sHOM-colonized *Il10*$^{-/-}$ mice (Figures 3K–3O). These results suggest that ectopic colonization of oral Enterobacteriaceae can trigger colitis in genetically susceptible hosts.

Oral Pathobionts Induce Colitis by Way of Activation of Inflammasome-Mediated IL-1β Secretion by Intestinal Mononuclear Phagocytes

Inflammasome-mediated secretion of IL-1β plays a central role in the pathogenesis of commensal pathobiont-driven IBD in mice (Seo et al., 2015). Likewise, patients with periodontitis have elevated levels of IL-1β (Park et al., 2014). Consistent with these observations, LOM-colonized *Il10*$^{-/-}$ mice displayed more prominent inflammasome-associated molecular signatures (e.g., IL-1β) compared with the GF control or the HOM-colonized group (Figure 4A; Table S2). To identify the cellular source of IL-1β, we next explored IL-1β-producing cells in colonic *lamina propria* (LP) cells of sHOM- or sLOM-colonized *Il10*$^{-/-}$ mice. As shown in Figures 4B and 4C, IL-1β-producing cells were significantly increased in sLOM-colonized *Il10*$^{-/-}$ mice compared with sHOM-colonized or control GF *Il10*$^{-/-}$ mice. Most IL-1β-producing cells were identified as inflammatory macrophages (Ly6C^{lo}MHC-II^{hi}CD64^{hi}) (Figures 4B–4D). Next we determined the extent to which IL-1β induced by gut colonization with oral pathobionts is involved in the pathogenesis of colitis. To this end, we used the DSS-induced colitis model in sHOM- and sLOM-colonized gnotobiotic mice and inhibited IL-1β signaling by administering the IL-1 receptor antagonist anakinra. Similar to *Il10*$^{-/-}$ mice, sLOM-colonized mice developed significantly more severe colitis when challenged with DSS (Figures 4E–4G). Anakinra treatment markedly attenuated colitis in sLOM-colonized mice, indicating the pivotal role of IL-1β in oral pathobiont-driven gut pathology (Figures 4E–4G). Next we validated the ability of each oral pathobiont strain to induce IL-1β secretion by macrophages. Oral pathobionts isolated from LOM induced robust production of IL-1β in bone marrow-derived macrophages (BMDMs) and colonic LP cells, unlike those isolated from HOM. Of note,

neither Enterobacteriaceae (*E. coli* strains SK460 and SK461) nor other Gram-negative strains (*Bacteroides thetaiotaomicron*, *B. uniformis*, and *B vulgatus*) isolated from the gut were able to induce IL-1β secretion (Figure 4H). Consistently, colonization of these gut-derived *E. coli* and *Bacteroides* strains did not lead to development of colitis in GF *Il10*$^{-/-}$ mice (Figure S3). Thus, IL-1β induction capacity may be a hallmark of colitogenic oral pathobionts.

Although we showed that gut colonization by oral pathobionts could elicit development of colitis in gnotobiotic mice, it remains possible that this occurs only in the absence of commensal microbes with immune-regulatory functions. To determine whether gut colonization by oral pathobionts is sufficient to exacerbate intestinal inflammation in the presence of competing microbes, we exogenously colonized conventional specific pathogen-free (SPF) mice with *K. aerogenes* strain SK431, the most abundant bacterium within LOM, in the DSS-induced colitis model (Figure 4I). Consistent with the gnotobiotic mouse experiments, gut colonization by *K. aerogenes* worsened DSS-induced colitis in SPF mice (Figures 4J–4L). Anakinra treatment was able to reverse the intestinal inflammation that resulted from *K. aerogenes* colonization (Figures 4J–4L). These results imply that ectopic gut colonization by oral pathobionts, such as *K. aerogenes*, is sufficient to exacerbate colitis by activation of IL-1 signaling. We next determined which inflammasome proteins are involved in IL-1β induction by oral pathobionts. Induction of mature IL-1β secretion by *K. aerogenes*-stimulated BMDMs was diminished or reduced in the absence of *Nlrp3*, *Pycard* (encodes ASC), *Casp1*, and *Casp11* (Figure S4A). Given that caspase−11 acts upstream of the NLRP3 inflammasome (Rathinam et al., 2012), this result indicates that the oral pathobiont *K. aerogenes* likely induces IL-1β production via caspase−11-mediated, non-canonical inflammasome activation. The Aim2 inflammasome also appears to be partially involved (Figure S4A). Consistent with this *in vitro* observation, *K. aerogenes* colonization did not exacerbate colitis in mice lacking *Nlrp3*, *Pycard*, *Casp1*, or *Casp11* (Figures S4B–S4D). Intestinal epithelial cells (IECs) are known to express various inflammasome proteins, including NLRP3 and caspase−11, and can produce inflammasome-related pro-inflammatory cytokines, such as IL-18 (Elinav et al., 2011; Knodler et al., 2014). Although IECs mainly produce IL-18 as a result of inflammasome activation and are not likely a source of IL-1β (Knodler et al., 2014), it has been reported that IECs can secrete mature IL-1β (Liu et al., 2017). Hence, oral pathobionts may activate the inflammasomes in IECs as well as macrophages. To address this possibility, we stimulated human cancer-derived IEC line T84 cells and primary mouse colonoids with oral pathobionts and symbionts. As a positive control, we used *Salmonella enterica* Typhimurium, which is known to activate the inflammasome in IECs (Knodler et al., 2014). Unlike macrophages, none of the bacterial strains, except *Salmonella*, induced secretion of mature IL-1β or IL-18 from T84 cells or mouse colonoids (Figures S4E–S4G). Taken together, oral pathobionts, such as *K. aerogenes*, upon gut colonization, enhance intestinal inflammation through activation of inflammasome-mediated IL-1 signaling in macrophages.

Oral Pathobiont-Reactive T Cells Arise in the Oral Cavity during Periodontitis

In addition to delivery of oral pathobionts to the gut, periodontitis could affect the severity of colitis in an immunological manner. In this regard, we found a significant accumulation of

Th17 and Th1 cells in the colonic mucosa of ligature-DSS mice compared with mice with only DSS colitis (Figures 1G–1M). Because the acute colitis model may lack a sufficient time span to develop memory T cell responses in the gut, we hypothesized that these T cells arise in the oral mucosa and transmigrate to the gut. To address this hypothesis, we first characterized the immune responses elicited by periodontitis in the oral cavity. We found that $CD3^+CD4^+CD44hiCD62L-$ effector memory T (TEM) cells accumulated in the cervical lymph nodes (cLNs), which drain the oral cavity following development of periodontitis (Figures 5A–5C). These TEM cells expressed $ROR\gamma t^+$ and produced robust amounts of IL-17A while producing limited amounts of IFN-γ and IL-10, indicating that oral TEM cells associated with periodontal disease exhibit a Th17 phenotype (Figures 5D–5F). To determine the antigen specificity of oral TEM cells, cLN $CD4^+$ T cells were stimulated with oral bacterial antigen-pulsed dendritic cells (DCs). As shown in Figure 5G, cLN $CD4^+$ T cells isolated from control mice did not recognize oral commensal antigens, whereas cLN $CD4^+$ T cells isolated from ligature mice responded to oral commensal antigens (Figure 5G). cLN $CD4^+$ T cells isolated from ligature mice responded more vigorously to oral bacterial antigens isolated from ligature mice than those isolated from healthy mice (Figure 5G). To identify the specific bacteria that activate oral Th17 TEM cells, we used single strains of bacteria normally associated with a healthy oral mucosa, an inflamed oral mucosa during periodontitis, and the gut mucosa. Oral TEM cells were reactive to *Klebsiella*/*Enterobacter* spp., all of which accumulated in the inflamed oral mucosa (Figure 2C). In contrast, neither oral bacteria typically found in a healthy oral cavity nor bacteria isolated from the gut mucosa activated oral TEM cells (Figure 5H). These results suggest that periodontitis induces generation of oral pathobiont-specific Th17 TEM cells. Of note, generation of oral pathobiont-specific Th17 TEM cells during periodontitis was significantly blunted, but not eradicated, in $IL\text{-}1R^{-/-}$ mice (Figure S5). Thus, oral pathobiont-induced IL-1β signaling may, at least in part, be involved in generation of Th17 cells.

Immune cells in cLNs are known to transmigrate to extra-oral lymphoid organs, including the gut (Morton et al., 2014). Therefore, as hypothesized earlier, it is possible that oral pathobiont-specific Th17 TEM cells arising from periodontitis can transmigrate to the gut. Consistent with this notion, oral Th17 TEM cells express α4β7 and CCR9, which regulate T cell homing to the intestine (Briskin et al., 1997; Johansson-Lindbom et al., 2005; Mora et al., 2003; Figures S6A and S6B). To evaluate the pathogenic capacity of oral Th17 TEM cells in the gut, we adoptively transferred cLN-derived TEM cells into gnotobiotic $Rag1^{-/-}$ mice (Figure 5I). To this end, GF $Rag1^{-/-}$ mice were reconstituted with sLOM or sHOM for 14 days (Figure 5I). No overt inflammation (fecal Lcn2) was observed as a result of colonization by either bacterial cocktail (Figure 5J). After 14 days of reconstitution, oral TEM cells (isolated from the cLNs of ligature mice) were adoptively transferred into gnotobiotic $Rag1^{-/-}$ mice. Consistent with antigen specificity *in vitro* (Figure 5H), adoptive transfer of oral TEM cells elicited development of colitis in sLOM-colonized $Rag1^{-/-}$ mice (Figures 5J–5L). In contrast, sHOM-colonized $Rag1^{-/-}$ mice did not develop colitis as a result of adoptive transfer of oral TEM cells (Figures 5J–5L). Importantly, transferred oral TEM cells failed to expand in the colonic mucosa of sHOM-colonized mice, whereas these cells proliferated in mice colonized with sLOM, suggesting that antigen-specific expansion

of oral TEM cells may be required for induction of colitis (Figures 5M and 5N). Consistent with this notion, oral TEM cells isolated from healthy mice, which do not react with HOM or LOM (Figure 5G), could not induce colitis in mice colonized with sHOM or sLOM (Figures S6C–S6E). Although oral pathobiont-reactive TEM cells exhibited Th17 phenotypes when they arose in the oral cavity (Figures 5D–5H) and expanded in the gut after transmigration (Figures 5O–5P), it remains unclear whether Th17 phenotypes are crucial for induction of inflammation after transmigrating to the gut. Hence, we used IL-17A-EGFP reporter mice and sorted IL-17A-producing TEM cells (EGFP$^+$ cells) and TEM cells that do not produce IL-17A (EGFP−) from cLNs (day 14 ligature-induced periodontitis) (Figure S7A). Sorted IL-17A-EGFP$^+$ and IL-17A-EGFP− oral TEM cells were then transferred into *Rag1*$^{-/-}$ recipient mice colonized with oral pathobionts (Figure S7B). As expected, transfer of IL-17A-EGFP$^+$ but not IL-17A-EGFP− oral TEM cells elicited development of colitis (Figures S7C–S7F). These results indicate that oral pathobiont-reactive Th17 TEM cells may contribute to development or exacerbation of intestinal inflammation when they were able to transmigrate to the gut.

Orally Primed T Cells Transmigrate to the Gut Mucosa

To confirm transmigration of oral T cells to the gut following development of periodontitis in immune-competent animals, we used Kaede transgenic mice (Tomura et al., 2008). All cell types in Kaede mice express the photoconvertible Kaede-Green fluorescent protein. When the photoconvertible protein is exposed to violet light, the protein changes its color from Kaede-Green to Kaede-Red (Tomura et al., 2008). This tool can be used to track cellular movement *in vivo* by analyzing the expression of Kaede-Red fluorescent protein in the destination organ. We first examined migration of T cells from cLNs to the gut under homeostatic conditions. The cLNs of Kaede transgenic (Tg) mice were exposed to violet light. Then the presence of Kaede-Red+CD3$^+$CD4$^+$ T cells in cLNs, mesenteric lymph nodes (mLNs), and colonic LP (cLP) was analyzed (Figure 6A). More than 40% of T cells in cLNs were converted by a short-term exposure to violet light (Figure 6A). Kaede-Red$^+$ cells translocated from the cLNs and were replaced by incoming Kaede-Green$^+$ cells within 7 days (steady-state leukocyte circulation), as reported previously (Morton et al., 2014; Figure 6A). Kaede-Red$^+$ cells were detected in mLNs on day 7, whereas none of these cells were present immediately after (1.5 h) photoconversion (Figure 6A), suggesting that T cells in cLNs can migrate to the gut under physiological conditions. In contrast to mLNs, no Kaede-Red+CD4$^+$ T cells were detected in the cLP (Figure 6A). Next we assessed the effect of gut inflammation on homing of oral T cells to the gut. Oral ligatures were placed into Kaede Tg mice, and after 14 days, the cLNs were irradiated with violet light, followed by DSS treatment 1 day later (Figure 6B). Neither ligature nor DSS colitis alone resulted in migration of orally primed T cells to the cLP (Figures 6B–6D). In contrast, increased numbers of Kaede-Red+CD4$^+$ T cells were detected in the cLP of DSS-treated mice with oral ligatures (Figures 6B–6D). Kaede-Red+CD4$^+$ T cells in the colonic mucosa showed predominantly Th17 (RORγt$^+$ and RORγt$^+$T-bet$^+$) phenotypes and limited numbers of Foxp3$^+$ cells (Figures 6E and 6F). Thus, orally primed T cells are capable of transmigrating to the gut mucosa.

Orally Primed T Cells Display Colitogenic Capacity in the Gut

To validate the colitogenic capacity of Kaede-Red+CD3$^+$CD4$^+$ T cells in the gut, we purified Kaede-Red+CD3$^+$CD4$^+$ T cells isolated from the cLP of Ligature-DSS mice and then adoptively transferred these cells into SPF *Rag1*$^{-/-}$ mice (Figure 6G). Purified Kaede-Green+CD3$^+$CD4$^+$ T cells isolated from the cLP of DSS-treated mice were used as a control (Figure 6G). Contrary to our expectations, adoptive transfer of Kaede-Red+CD3$^+$CD4$^+$ T cells did not elicit development of colitis in SPF *Rag1*$^{-/-}$ mice because fecal Lcn2 levels were not elevated during the 8-week period (Figure 6G). We theorized that this phenotype is due to the inability of the gut-resident microbiota to activate transferred oral pathobiont-reactive T cells. In other words, expansion of oral pathobionts in the gut is required for activation of oral bacterium-reactive T cells in the gut. We tested this hypothesis by colonizing mice with the oral pathobiont *K. aerogenes*, mimicking increased abundance of oral pathobionts in the gut. Based on the calculation that a typical person swallows an estimated 1.5 × 1012 oral bacteria per day (1.5 × 1012/day/70 kg 0.53 × 109/gavage/25-g mouse) (Schmidt et al., 2019), we inoculated mice with 1 × 109 *K. aerogenes* 3 times per week for 4 weeks. Gut colonization with *K. aerogenes* did not elicit gut inflammation (as measured by fecal Lcn2) in sham control *Rag1*$^{-/-}$ mice or *Rag1*$^{-/-}$ mice reconstituted with Kaede-Green+CD3$^+$CD4$^+$ T cells (Figures 6G–6K). On the other hand, oral gavage with *K. aerogenes* resulted in development of severe colitis in *Rag1*$^{-/-}$ mice reconstituted with Kaede-Red+CD3$^+$CD4$^+$ T cells (Figures 6G–6K). Notably, the gut pathology of mice transferred with Kaede-Red+CD3$^+$CD4$^+$ T cells was significantly attenuated by treatment with the IL-1R antagonist anakinra (Figures 6L–6O). This was accompanied by a reduction in the total number of CD4$^+$ T cells as well as RORγt$^+$ and RORγt$^+$T-bet$^+$ Th17 cells in the colon (Figures 6P–6S). Consistent with this result, secretion of IL-17A and IFN-γ by colonic CD4$^+$ T cells was also decreased (Figure 6T). These results indicate that the population of oral microbiota-reactive T cells, which are enriched with pathogenic Th17 cells, could transmigrate to the gut. Upon arrival in the gut, oral microbiota-reactive Th17 cells may expand by reacting to their cognate antigens (i.e., ectopically colonized oral pathobionts), promoting development of colitis. Gut mucosal IL-1β induced by oral pathobionts may also be involved in activation and/or expansion of the transmigrated oral T cells.

Gut Transmigration of Orally Primed T Cells Exacerbates Colitis

So far, we have demonstrated that oral pathobiont-reactive Th17 cells that arise during periodontitis have a colitogenic capacity. However, the extent to which gut-transmigrated oral Th17 cells are involved in the pathogenesis of colitis remains unclear. To address this question, we used a parabiosis model. As shown in Figure 7A, periodontitis was induced in CD45.2$^+$ WT C57BL/6 mice (donors of orally primed T cells). After 14 days of oral ligature insertion, these mice were surgically connected to congenic CD45.1$^+$ mice by parabiosis. After 1 week, colitis was induced only in CD45.1$^+$ mice by oral gavage of DSS. These mice were also orally challenged with *K. aerogenes* to supply cognate antigens to gut-migrated oral T cells. CD45.1$^+$ mice connected to periodontitis CD45.2$^+$ mice (group 4) developed significantly more severe colitis compared with CD45.1$^+$ mice connected to healthy mice (Group 3) when challenged with DSS/*K. aerogenes* (Figures 7B–7D). In group 4 mice, we observed massive migration of CD45.2+CD3$^+$CD4$^+$ T cells (derived from connected

periodontitis mice) into the colonic mucosa of CD45.1$^+$ mice (Figures 7B–7D). These gut-migrated T cells, which are derived from periodontitis mice, revealed RORγt$^+$ and RORγt +T-bet$^+$ Th17 cell phenotypes and, indeed, produced robust amounts of IL-17A and IFN-γ (Figures 7E–7J). Importantly, the connection to periodontitis mice did not worsen DSS colitis nor increase gut migration of Th17 cells associated with periodontitis mice when *K. aerogenes* was not supplied (group 5), indicating that the presence of oral pathobionts in the gut is a prerequisite for expansion of orally primed Th17 cells and the subsequent induction of intestinal inflammation by these cells in the gut (Figures 7B–7J).

DISCUSSION

In this study, we found that periodontal inflammation contributes to the pathogenesis of IBD. Inflammation in the oral mucosa fosters blooms of Enterobacteriaceae, such as *Klebsiella* and *Enterobacter* spp., and ectopic gut colonization of these bacteria plays a crucial role in exacerbation of intestinal inflammation. It is noteworthy that oral pathobionts do not colonize the gastrointestinal tract of healthy individuals (Figure 2E). This evidence suggests that at least two conditions must be met for oral pathobionts to ectopically colonize the gut. First, the colonization resistance of gut-resident microbiota must be disrupted, enabling the oral microbes to invade the gut. In the current study, gut inflammation perturbed colonization resistance mediated by the resident microbiota, making it possible for ingested oral pathobionts to outcompete and displace the resident bacteria. Moreover, Enterobacteriaceae are metabolically adapted to thrive in the inflammatory milieu. Hence, intestinal inflammation favors the growth of Enterobacteriaceae, including bacteria translocated from the oral mucosa (Kitamoto et al., 2020; Winter et al., 2013; Zhu et al., 2018). However, loss of colonization resistance or gut inflammation alone does not facilitate ectopic gut colonization by oral pathobionts. The second condition that must be met is oral inflammation. There likely is a threshold for the number of ingested oral pathobionts that must be reached for them to successfully transition from the oral cavity to the gut. Periodontal inflammation is therefore essential because it raises the abundance of oral pathobionts and increases the likelihood of successful passage through the acidic environment encountered in the stomach. Alternatively, neutralization of gastric acid or inhibition of acid secretion could promote ectopic colonization of oral bacteria in the gut. For example, it has been reported that use of proton pump inhibitors, which reduce production of gastric acid, leads to increased colonization of mouth-resident bacteria in the gut (Imhann et al., 2016; Jackson et al., 2016). Consistent with this observation, it has been reported that gastric acid inhibitors worsen clinical outcomes in IBD (Juillerat et al., 2012; Shah et al., 2017).

Ectopically colonized oral pathobionts may be involved in exacerbation of colitis through the synergistic effects of two distinct mechanisms: activation of mucosal inflammatory responses (direct) and by serving as cognate antigens for transmigrated oral T cells (indirect). Inflammasome activation and subsequent induction of IL-1β by oral pathobionts likely plays a central role in the first mechanism; i.e., direct induction of colitis in the gut (Figure 4; Figure S4). In parallel, ectopically colonized oral pathobionts are required for expansion of gut-transmigrated oral TEM cells, possibly through antigen-specific proliferation (Figures 5, 6, and 7; Figure S6). Of note, these two mechanisms may act

synergistically. IL-1β induced by ectopically colonized oral pathobionts may also contribute to activation and/or expansion of oral TEM cells in the gut mucosa (Figures 6L–6T). Thus, it is possible that prevention of ectopic gut colonization by oral pathobionts not only reduces the abundance of colitogenic pathobionts but also attenuates expansion of colitogenic T cells in the gut.

$CD4^+$ T lymphocytes are believed to play a crucial role in the pathogenesis of IBD (Neurath, 2014). In IBD patients, Th1, Th17, or Th1/Th17 combined phenotypes of $CD4^+$ T cells are found accumulated in the intestinal mucosa (Calderón-Gómez et al., 2016; Hegazy et al., 2017). These pathogenic $CD4^+$ T cells are reactive to resident bacteria (Calderón-Gómez et al., 2016; Hegazy et al., 2017; Shen et al., 2008). However, the mechanism by which bacterium-reactive pathogenic T cells arise in the context of IBD remains incompletely understood. It has been reported that colonization by gut-resident microbiota elicits development of bacterium-specific tolerogenic and effector T cell responses. Specific gut microbes, such as *Clostridium* clusters XlVa and IV or *Bacteroides* strains (Atarashi et al., 2011, 2013; Faith et al., 2014; Round et al., 2011), are known to induce peripheral $Foxp3^+$ Treg cells in the gut; therefore, these bacteria do not elicit pathogenic T cell responses. Colonization by segmented filamentous bacteria (SFBs) elicits differentiation of $ROR\gamma t^+$ Th17 effector cells (Ivanov et al., 2009; Xu et al., 2018). However, these SFB-specific Th17 cells are homeostatic effector cells and do not cause intestinal inflammation (Xu et al., 2018). Gut colonization by a known intestinal pathobiont, *Helicobacter hepaticus*, results in differentiation of Foxp3+$ROR\gamma t^+$ Treg and $ROR\gamma t^+$ Th17 cells (Xu et al., 2018). Treg cells limit activation of Th17 cells under homeostatic conditions (in wild-type [WT] animals); hence, colonization by *H. hepaticus* fails to elicit intestinal inflammation. Thus, the gut microenvironment is conducive to development of tolerogenic immunity against commensal microbiota. Consistent with this notion, in this study, $CD4^+$ T cells isolated from the colonic mucosa of mice with acute DSS colitis, which may contain microbiota-specific memory T cells, were enriched with $Foxp3^+$ Tregs and, therefore, not colitogenic ($Kaede\text{-}Green^+$ T cells in Figures 6E–6K). Thus, the microbiota-specific $CD4^+$ T cells that arise during acute gut inflammation likely retain their tolerogenic phenotype. On the other hand, oral pathobiont-reactive T cells that arise during periodontitis are colitogenic. These differences may be due to the distinct immunological properties of the oral and gastrointestinal mucosa. Although the reason why the tolerogenicity of these two mucosal sites differs remains to be explored, the distinct microbial and immunological milieus may, in part, explain this difference. For example, the gut mucosa is colonized by butyrate-producing bacteria, such as *Clostridium* strains, and this microbial metabolite shapes tolerogenic immunity by promoting generation of $Foxp3^+$ Treg cells as well as inducing secretion of IL-10 by mucosal mononuclear phagocytes (Furusawa et al., 2013; Singh et al., 2014). However, the availability of butyrate may be limited in the oral mucosa and periodontium because of the absence of butyrate-producing bacteria as well as appropriate substrates (e.g., dietary fibers). Likewise, the gut mucosa has at its disposal alternative immune mechanisms that limit generation of microbiota-reactive effector T cells. For example, a subset of innate major histocompatibility complex (MHC) class II-expressing lymphoid cells inhibits proliferation of microbiota-specific T cells (Hepworth et al., 2015). The oral mucosa and gingiva likely lack these multi-layered tolerogenic mechanisms that are present in the gut. Consequently,

acute inflammation in the oral mucosa can trigger generation of microbiota-reactive pathogenic T cells.

Th17 cells play a key pathogenic role in commensal bacterium-driven inflammation in the oral cavity in mice and humans (Beklen et al., 2007; Cheng et al., 2016; Dutzan et al., 2018; Eskan et al., 2012; Moutsopoulos et al., 2014; Takahashi et al., 2005). Consistent with this concept, we found that ligature-induced periodontal inflammation causes proliferation of oral commensal pathobiont-reactive Th17 cells. However, the commensal-specific Th17 cells that naturally occur in the gut (Atarashi et al., 2015; Ivanov et al., 2009; Shaw et al., 2012; Xu et al., 2018) are not pathogenic (Ono et al., 2012). It has been reported that Th17 cells undergo pathogenic conversion under certain circumstances in the gut and give rise to IFN-γ-producing Th1-like $CD4^+$ T cells. These ex-Th17 cells are pathogenic and cause severe intestinal inflammation (Ahern et al., 2010; Harbour et al., 2015). In this study, we found that the oral commensal pathobiont-specific TEM cells that arise during periodontitis had a $ROR\gamma t^+$ T-bet− Th17 phenotype and indeed produced IL-17A but not IFN-γ (Figures 5A–5F; Figure S7A). However, after arriving at the gut mucosa, these cells could produce IFN-γ (Figure S7F). Thus, functional conversion of oral Th17 TEM cells into the IFN-γ-producing Th17/Th1 mixed phenotype may be involved in the pathogenesis of colitis elicited by oral T cells.

Collectively, our results provide evidence that the oral and gastrointestinal mucosae are microbiologically and immunologically connected. Thus, optimal oral care (e.g., removal of pathogenic oral biofilms and reduction of periodontal inflammation) could reduce the risk of IBD by limiting the expansion of pathogenic effector T lymphocytes and their reactive antigens. Likewise, inhibition of migration of oral TEM cells to the gut might be an alternative strategy used to block the pathogenic mouth-gut axis in the context of IBD.

STAR★METHODS

RESOURCE AVAILABILITY

Lead Contact—Further information and requests for resources and reagents should be directed to and will be fulfilled by the Lead Contact, Nobuhiko Kamada (nkamada@umich.edu).

Material Availability—Bacterial strains isolated/identified in this study are available from the Lead Contact with a completed Materials Transfer Agreement.

Data and Code Availability—Raw sequences are available via NCBI Short-Read Archive with BioProject number PRJNA631055

EXPERIMENTAL MODEL AND SUBJECT DETAILS

Mice—Eight- to twelve-week-old female and male mice were used. Specific pathogen-free (SPF) C57BL/6 were housed in the Animal Facility at the University of Michigan. Germ-free (GF) C57BL/6 mice were housed in flexible film isolators at the University of Michigan Gnotobiotic Animal Facility. The absence of microbes in GF mice was verified weekly by aerobic and anaerobic microbial culture and microscopic analysis of stained cecal contents.

For gnotobiotic mice experiments, GF mice were reconstituted with consortia of identified bacterial strains. Gnotobiotic mice were housed in positive-pressure individually ventilated cages (IVC) (ISOcage P, Techniplast) per each condition to prevent cross-contamination among the different experimental groups (Hecht et al., 2014; Nagao-Kitamoto et al., 2016; Paik et al., 2015). GF and gnotobiotic mice were given autoclaved distilled water, provided *ad libitum*, and sterile animal chow (rodent breeder diet 5013 (LabDiet)). SPF mice were fed a sterilized laboratory rodent diet 5L0D (LabDiet). All animals were handled in accordance with the protocols approved by the Institutional Animal Care and Use Committee (IACUC) at the University of Michigan and were in concordance with ARRIVE guidelines for preclinical studies (Kilkenny et al., 2010). Details of mouse strains used in this study can be found in the Key Resources Table (Adachi et al., 1998; Chen et al., 2011; Franchi et al., 2006; He et al., 2016; Man et al., 2017; Seo et al., 2015).

METHOD DETAILS

Isolation and identification of bacteria—For the isolation of oral bacteria, ligatures were collected from mice 3 h post ligature placement (healthy oral microbiota; HOM) or 14 days post ligature placement (ligature-associated microbiota; LOM) and resuspended in sterile cold-PBS. Then, the bacterial suspensions were spread onto brain heart infusion agar plates containing 5% FBS or MacConkey agar plates and incubated overnight under aerobic conditions at 37°C. Bacterial DNA was extracted from each single colony and the identity of individual isolates was verified by Sanger sequencing of the V1-V9 regions of 16S rRNA genes. The following primer set was used for amplifications: Eubacteria16S_8F; 5′-AGAGTTTGATCCTGGCTCAG−3′ and Eubacteria16S_1492R; 5′-GGTTACCTTGTTACGACTT−3′. Whole genome sequencing was performed using the Illumina MiSeq (500v2) platform. 150 bp-long high quality paired-end reads were assembled into contigs by SPAdes 3.13.0 (Bankevich et al., 2012) and the assembled contigs were annotated by RAST (Seemann, 2014). Isolates were identified by BLAST using the rpoB gene sequences. Gut commensal *Bacteroides* strains (*B. thetaiotaomicron, B. uniformis,* and *B vulgatus*) were obtained from Dr. Thaddeus Stappenbeck (Bloom et al., 2011).

Isolation of lymphocytes—For the cell isolation from lymph nodes, the dissected lymph nodes were pressed through a 100 μm nylon filter using the black rubber end of a 1-mL syringe plunger, and then digested by complete RPMI containing 400 U/mL type 3 collagenase and 0.01 mg/mL DNase I (Worthington Biochemical, Lakewood, NJ) for 30 min at 37°C. Then, if needed, the EasySep Mouse $CD4^+$ T Cell Isolation Kit (STEMCELL Technologies, Vancouver, BC, Canada) was used to purify the $CD4^+$ T cells. For the lamina propria (LP) cell isolation from colon, the dissected mucosal tissue was incubated in calcium and magnesium-free Hank's balanced salt solution (HBSS) (Life Technologies, Carlsbad, CA) containing 1.5% heat-inactivated fetal bovine serum (FBS) (Life Technologies) and 1 mM dithiothreitol (Sigma-Aldrich) to remove mucus. Epithelial cells were removed by incubation in HBSS containing 1 mM EDTA (Quality Biological, Gaithersburg, MD) at 37°C for 30 min. After washing with HBSS, remaining tissues were collected and incubated, with agitation, in HBSS containing 400 U/mL type 3 collagenase and 0.01 mg/mL DNase I (Worthington Biochemical) for 90 min at 37°C. The digested cell fraction was pelleted, re-

suspended in a 40% Percoll solution (GE Healthcare Life Sciences, Pittsburgh, PA), layered on top of a 75% Percoll solution, and centrifuged at 2000 rpm for 20 min at room temperature. Viable lamina propria mononuclear cells (LPMCs) were recovered from the discontinuous gradient interface.

Immune cell analysis—For myeloid cell analysis by conventional flow cytometry, isolated immune cells were labeled with DAPI and stained with anti-CD45, IL-1β, Ly6C, MHCII, CD11c, and CD64 antibodies. For the surface staining in the lymphoid cell analysis, anti-CD3e, CD4, CD44, CD62L, CD25, α4 β7, and CCR9 antibodies were used, accordingly. For intranuclear staining, cells were permeabilized and stained with T-bet, RORγt, and Foxp3 using the Foxp3/Transcription Factor Staining Buffer Kit (Tonbo Biosciences), according to the manufacturer's instructions. All data were collected on a BD LSRFortessa and BD Celesta FACSAria II (BD Biosciences) and analyzed with FlowJo software (BD Biosciences).

Mass cytometry (CyTOF) analysis—We validated a 40-marker panel for CyTOF murine immune profiling. The lanthanide metals were acquired from Fluidigm and conjugated to antibodies using a maxpar antibody labeling kit. The final concentration of the metal-tagged antibody was determined by measuring the absorbance at 280 nm. The immune cells were stained with 1.25 μM live/dead stain (Cell-ID Cisplatin−195Pt diluted in serum-free media from 500 mM stock). Free cisplatin was quenched by washing the cells with serum-containing media. The metal-tagged antibody cocktail was made in CyFACS buffer and added to the cells in the presence of TruStain FcX (Biolegends) and incubated on ice for 60 min. Then, cells were fixed with 1.6% PFA and permeabilized with eBioscience permeabilization buffer for 30 min. The cells were then stained with 50 μL of intracellular staining metal-tagged antibody cocktail (made in eBioscience permeabilization buffer) at RT for 60 min. Data were acquired using the CyTOF Helios system (Fluidigm). After clones and channels are optimized for each antibody, we performed a viSNE analysis using Cytobank, which allows us to map high-dimensional data onto two dimensions (Amir et al., 2013).

Quantitative Real-Time PCR—Colonic tissue samples were harvested, and RNA was extracted using E.Z.N.A. Total RNA Kit I (Omega Bio-tek). cDNA was reverse transcribed using a High Capacity RNA-to-cDNA Kit (Thermo Fisher Scientific) and used for SYBR Green Gene-Expression Assay (Thermo Fisher Scientific) on an ABI 7900HT analyzer. Primer sequences used in this study can be found in the Key Resources Table (Arfi et al., 2011; Burr et al., 2006; Curtis et al., 2014; Ellett et al., 2009; Lu et al., 2017; Miyata et al., 2016; Okumura et al., 2016; Pakala et al., 2010; Sand et al., 2018; Seregin et al., 2017; Wang et al., 2017; Watanabe et al., 2009).

Experimental periodontitis model—Murine periodontitis was induced by ligature placement (Jiao et al., 2013; Marchesan et al., 2018). Mice were anesthetized with ketamine/xylazine and silk sutures (100 μm diameter; SUT−15−1; Roboz Surgical Instrument Co.) were inserted between the first and second maxillary molars on contralateral right and left sides. Both ends of the suture string were knotted to prevent ligature loss. The silk sutures

remained in place for 14 days or 3 h (sham control). Mice were euthanized at the end points of each experiment. Inserted sutures were collected from the euthanized mice and used for microbial analyses. Block biopsies from the maxillae were fixed in 10% formalin. The fixed tissues were then used to check bone loss by micro–computed tomography (micro-CT) (Jiao et al., 2013).

Dextran sulfate sodium (DSS)–induced colitis model—For DSS-induced colitis, SPF C57BL/6 WT mice with ligatures (day 14) were treated with 1.5% DSS for 5 days. The animals were monitored for weight loss (0, none; 1, 1%–5%; 2, 5%–10%; 3, 10%–20%; 4, > 20%), stool consistency (0, normal stool; 2, loose stool; 4, diarrhea), and hemoccult (0, normal; 2, hemoccult positive; 4, gross blood) during the course of experiments, and these parameters were used to compute the disease activity index. Mice were sacrificed on day 7 and histological scores were assigned in a blind manner by a trained pathologist evaluating the following set of variables (Cooper et al., 1993; Klopfleisch, 2013): severity of inflammation (0, none; 1, low density confined to mucosa; 2, moderate or higher density in mucosa and/or low to moderate density in mucosa and submucosa; 3, high density in submucosa and/or extension to muscularis; 4, high density with frequent transmural extension), and extent of epithelial/crypt damage (0, none; 1, basal 1/3; 2, basal 2/3; 3, crypt loss; 4, crypt and surface epithelial destruction). Each variable was multiplied by a factor reflecting the percentage of the colon involved (1, 0%–25%; 2, 26%–50%; 3, 51%–75%; 4, 76%–100%). An overall score was obtained by summing the scores assigned to each variable. For oral pathobiont colonization experiments, mice received 2.0% DSS for 5 days followed by regular water for 2 days. The oral pathobiont SK431 (*K. aerogenes*) was used for oral challenge every day (1 × 109 CFU/dose). The IL-1R antagonist anakinra (50 mg/kg) or saline was i.p. injected into Ka-colonized mice every day. Histological analysis was performed as described above.

IL-10–deficient colitis model—GF *Il10*$^{-/-}$ mice were colonized with either HOM or LOM, and maintained for 56 days. For the experiments with synthetic oral communities, a mixture of 3 isolates from HOM (*Streptococcus salivarius, Streptococcus* sp. JS71, *and Staphylococcus xylosus*) or 5 isolates from LOM (*Klebsiella aerogenes, Klebsiella pneumonia, Klebsiella variicola, Enterobacter cloacae,* and *Enterobacter hormachaei*) was used (109 CFU of each strain per mouse). All mice inoculated with bacterial mixtures were housed in gnotobiotic isolators. Mice were sacrificed on day 56 and histological assessment was performed in a blind fashion by a trained pathologist using a previously described immune cell–driven colitis scoring system (Erben et al., 2014). Briefly, severity of inflammation was evaluated according to the following scale: (0, none; 1, minimal (lesions restricted to mucosa; lesions consist of minimal hyperplasia with minimal scattered inflammation); 2, mild (lesions affecting mucosa with infrequent submucosal extension; lesions consist of mild hyperplasia with mild inflammation ± minimal goblet cell loss, and/or erosions); 3, moderate (lesions affecting mucosa and submucosa; lesions consist of moderate hyperplasia with moderate inflammation ± few crypt abscesses, moderate goblet cell loss, and/or erosions); 4, severe (lesions affecting mucosa and submucosa; lesions consist of severe hyperplasia with multifocal severe inflammation ± several crypt abscesses, erosions/ulcerations, and/or irregular crypts/crypt loss); 5, marked (transmural lesions,

lesions consist of marked hyperplasia with marked inflammation, +/− multiple crypt abscesses, erosions/ulcerations, irregular crypts/crypt loss, and/or inflammation).

T cell responsiveness to bacterial antigens—For the isolation of $CD4^+$ T cells from cLN, cLNs were harvested from ligature mice (day 14) and the mouse $CD4^+$ T cell Isolation Kit (STEMCELL Technologies) was used to isolate cells from single cell suspensions prepared from the cLNs. For the preparation of the bone marrow–derived dendritic cells (BMDMs), murine bone marrow cells were cultured in the RPMI/10% FBS containing recombinant murine 10 ng/mL GM-CSF (PeproTech, Rocky Hill, NJ) for 6 days. Loosely attached DC cells were then collected using the biotin selection kit (STEMCELL Technologies) and enriched with biotinylated CD11c monoclonal antibody (Thermo Fisher Scientific, Waltham, MA). BMDCs were pulsed with heat-denatured bacterial antigens for 18 h at 37°C. Antigen-pulsed BMDCs and cLN-derived $CD4^+$T cells were co-cultured for 24 h at 37°C. Cytokines in supernatants were quantified by ELISA.

Kaede photoconversion—Kaede Tg mice were anesthetized with ketamine and xylazine. Lubricating ophthalmic ointment was placed in each eye to prevent dryness. The overlying fur around the cLN area was removed using a depilatory cream or an electric shaver. Following hair removal, the operating field was properly sterilized, as required by the rodent surgery guidelines and covered with a surgical drape. A skin incision was made in the depilated area (5–10 mm). The mice were placed on their backs with an aluminum foil blanket covering all but the depilated area, and violet light (LRD−0405 Collimated Diode Laser System; Laserglow Technologies, North York, ON, Canada) was shone (405 nm; peak power < 50 mW) onto the exposed area for a period of 1 min (50 mW direct exposure). In order for both LNs to be simultaneously exposed to violet light, we attached a lens to the laser, thus blurring the beam, and the laser head was positioned 5–20 cm above the mouse. Following photoconversion, the incision was closed with simple interrupted sutures (4.0 Vicryl, 1.5 metric; Ethicon, Somerville, NJ).

T cell transfer colitis model—GF *Rag1*$^{-/-}$ mice were colonized by either sHOM or sLOM for 14 days. $CD3^+CD4^+$CD44hiCD62LloCD25- TEM cells were isolated from the cLNs of ligature mice (day 14). Isolated TEM cells (2 × 105 cells/mouse) were then adoptively transferred into gnotobiotic (sHOM or sLOM) *Rag1*$^{-/-}$ mice and control GF *Rag1*$^{-/-}$ mice. *Rag1*$^{-/-}$ mice were maintained for 8 weeks post adoptive transfer. For experiments with Kaede mice, LPMCs were isolated from ligature and DSS-treated Kaede mice. Kaede-Red^+ or Kaede-$Green^+$ $CD3^+CD4^+$ T cells were then sorted by FACS and adoptively transferred into SPF *Rag1*$^{-/-}$mice (2 × 105 cells/mouse, i.v.), respectively. The negative control group received saline. The mice were monitored for 8 weeks post adoptive transfer. After 8 weeks, *K. aerogenes* SK431 (1 × 109 CFU/mouse) was administered orally 3 times per week for an additional 4 weeks. Histological assessment was performed in a blind fashion by a trained pathologist using the immune cell-driven colitis scoring system described above.

Parabiosis model—SPF $CD45.2^+$ mice were treated with oral ligatures for 14 days and then surgically attached to congenic $CD45.1^+$ mice. Briefly, 2 age-matched females

(CD45.1$^+$ and CD45.2+, respectively) were placed in the supine position. The hair on the left side of the mouse was placed on the left, and the hair on the right side of the mouse was placed on the right was thoroughly shaved starting about 1 cm above the elbow to 1 cm below the knee. Carprofen was given to the mice for analgesia. Using sterile, sharp scissors, longitudinal skin incisions were made on the shaved side of each animal, from 0.5 cm above the elbow to 0.5 cm below the knee joint. After making the incision, the skin from the subcutaneous fascia was gently detached by holding the skin up with a pair of curved forceps and separating the fascia with a second pair to create 0.5 cm of free skin. Surgical autoclips (9-mm, BD Biosciences) were used to join the skin of the two mice. Each pair of mice joined by parabiosis was housed in a cage (i.e., 2 mice (joined by parabiosis) per cage). During the 1-week recovery phase, the analgesic carprofen was given every 24 h for 2 days. One week after surgery, *K. aerogenes* (109 CFU/shot) and DSS (100 mg/shot), which allow oral pathobionts to colonize the gut by disrupting gut colonization resistance, were administered by oral gavage to recipient CD45.1$^+$ mice only, daily for 6 days.

Establishment of two-dimensional colonoids—Isolation of murine colonoid cultures was performed as previously described (Reed et al., 2019; Sato et al., 2009). Briefly, freshly isolated colons were treated with Cell Recovery Solution (Corning) for 5min followed by additional 30 min in ice-cold chelation buffer (50 mM EDTA/PBS) for 30 min with gentle inversion at 4°C. Colons were then shaken to dissociate crypt fraction. After centrifugation (400 g, 10min at 4°C), colonic crypts in the pellet were resuspended in complete enteroid medium (advanced DMEM/F12 based medium containing 50% LWRN condition media and 200 ng/ml of recombinant human EGF) and seeded on to collagen type IV-coated 48-well tissue culture plates until confluency was achieved (~24 h).

***In vitro* stimulation by bacteria—**To generate bone marrow-derived macrophages (BMDMs), BM cells were isolated from SPF WT C57BL/6 mice and cultured for 6 days with Iscove's Modified Dulbecco's Medium supplemented with 30% L929 supernatant. Colonic lamina propria (LP) cells were isolated from DSS-induced colitis mice. BMDMs or colonic LP cells were co-cultured with oral or gut bacterial strains (MOI = 5) for 3 h. Gentamicin (100 μg/ml) was then added and cells were further cultured for additional 16 h. For bacteria-epithelial cells (T84, mouse 2D colonoids) co-culture experiments, bacterial strains at MOI = 10 were used. Gentamicin (100 μg/ml) was added 3 h after co-culture, and cells were then incubated for additional 16 h. Culture supernatants were harvested, and cytokines were measured by ELISA. In some experiments, *Salmonella enterica* serovar Typhimurium strain SL1344 was used as a positive control (Franchi et al., 2012).

Microbiome analysis—For gut microbiome analysis, fecal samples were obtained from individual mice. For oral microbiome analysis, inserted silk sutures were collected. Genomic DNA was extracted by using a modified protocol of the DNeasy Blood & Tissue Kit (QIAGEN, Germantown, MD) (Nagao-Kitamoto et al., 2016). Microbiome analysis was performed at the Microbial Systems Molecular Biology Laboratory at the University of Michigan. 16S rRNA gene libraries were constructed using primers specific to the V4 region and processed using the Illumina MiSeq sequencing platform. Sequences were curated using the community-supported software program Mothur version 1.39.0 (Schloss et al., 2009).

Sequences were assigned to operational taxonomic units (OTUs) using a cutoff = 0.03 and classified against the Ribosomal Database Project (RDP) 16S rRNA gene training set (version 16) using a naive Bayesian approach with an 80% confidence threshold. Curated OTU sequence data were converted to relative abundance ± standard error of the mean (SEM). Linear discriminant analysis effect size (LEfSe) (Segata et al., 2011) was used to identify bacterial taxa that were differentially abundant, biologically consistent, and had the greatest effect size.

QUANTIFICATION AND STATISTICAL ANALYSIS

Unless otherwise stated in individual method sections above, all statistical analyses were performed using Prism 7 (GraphPad Software, San Diego, CA). Differences between two groups were evaluated using the Student t test (parametric) or Mann–Whitney *U* test (non-parametric). For a comparison of more than 3 groups, statistical analysis was performed using one-way ANOVA (parametric) or Kruskal–Wallis test (non-parametric), followed by the Bonferroni correction for parametric samples, or Dunn's test for non-parametric samples as a post hoc test. Survival analysis was performed using Kaplan–Meier curves, with comparisons between groups made using the log-rank test. Differences of $p < 0.05$ were considered significant in all statistical analyses. Statistically significant differences are shown with asterisks as follows: *; $p < 0.05$, **; $p < 0.01$, ***; $p < 0.001$ and ****; $p < 0.0001$; whereas, ns indicates comparisons that are not significant. Numbers of animals (n) used for individual experiments, details of the statistical tests used and pooled values for several biological replicates are indicated in the respective figure legends.

Supplementary Material

Refer to Web version on PubMed Central for supplementary material.

ACKNOWLEDGMENTS

The authors thank the University of Michigan Center for Gastrointestinal Research (NIH 5P30DK034933), the Host Microbiome Initiative, the Germ-Free Animal Facility, the Advanced Genomics Core, the Microbial Systems Molecular Biology Laboratory, the CyTOF core, and the Flow Cytometry Core for technical assistance and the In-Vivo Animal Core at the University of Michigan for histological evaluation. We also thank Meenal Mhaskar, Chithra K. Muraleedharan, Vicky Garcia-Hernandez, Miguel Quiros, Yoshiro Aoki, Yuping Zhang, Yasuyuki Hosono, Sergey S. Seregin, and Grace Y. Chen for experimental assistance. This work was supported by National Institutes of Health grants DK108901, DK119219, and AI142047 (to N.K.) and U01 DE029255 (to Y.L.L.), a JSPS Postdoctoral Fellowship for Research Abroad (to S.K., H.N.-K., and K.S.), an Uehara Memorial Foundation Postdoctoral Fellowship Award (to S.K. and K.S.), the Crohn's and Colitis Foundation (to H.N.-K., K.S., S.B., and N.I.), the University of Michigan Clinical and Translational Science Awards Program (UL1TR002240 to S.K.), and the Prevent Cancer Foundation (to S.K.).

REFERENCES

Abe T, and Hajishengallis G (2013). Optimization of the ligature-induced periodontitis model in mice. J. Immunol. Methods 394, 49–54. [PubMed: 23672778]

Adachi O, Kawai T, Takeda K, Matsumoto M, Tsutsui H, Sakagami M, Nakanishi K, and Akira S (1998). Targeted disruption of the MyD88 gene results in loss of IL-1- and IL-18-mediated function. Immunity 9, 143–150. [PubMed: 9697844]

Ahern PP, Schiering C, Buonocore S, McGeachy MJ, Cua DJ, Maloy KJ, and Powrie F (2010). Interleukin−23 drives intestinal inflammation through direct activity on T cells. Immunity 33, 279–288. [PubMed: 20732640]

Amir ED, Davis KL, Tadmor MD, Simonds EF, Levine JH, Bendall SC, Shenfeld DK, Krishnaswamy S, Nolan GP, and Pe'er D (2013). viSNE enables visualization of high dimensional single-cell data and reveals phenotypic heterogeneity of leukemia. Nat. Biotechnol 31, 545–552. [PubMed: 23685480]

Arfi A, Richard M, Gandolphe C, Bonnefont-Rousselot D, Thérond P, and Scherman D (2011). Neuroinflammatory and oxidative stress phenomena in MPS IIIA mouse model: the positive effect of long-term aspirin treatment. Mol. Genet. Metab 103, 18–25. [PubMed: 21353610]

Atarashi K, Tanoue T, Shima T, Imaoka A, Kuwahara T, Momose Y, Cheng G, Yamasaki S, Saito T, Ohba Y, et al. (2011). Induction of colonic regulatory T cells by indigenous Clostridium species. Science 331, 337–341. [PubMed: 21205640]

Atarashi K, Tanoue T, Oshima K, Suda W, Nagano Y, Nishikawa H, Fukuda S, Saito T, Narushima S, Hase K, et al. (2013). Treg induction by a rationally selected mixture of Clostridia strains from the human microbiota. Nature 500, 232–236. [PubMed: 23842501]

Atarashi K, Tanoue T, Ando M, Kamada N, Nagano Y, Narushima S, Suda W, Imaoka A, Setoyama H, Nagamori T, et al. (2015). Th17 Cell Induction by Adhesion of Microbes to Intestinal Epithelial Cells. Cell 163, 367–380. [PubMed: 26411289]

Atarashi K, Suda W, Luo C, Kawaguchi T, Motoo I, Narushima S, Kiguchi Y, Yasuma K, Watanabe E, Tanoue T, et al. (2017). Ectopic colonization of oral bacteria in the intestine drives TH1 cell induction and inflammation. Science 358, 359–365. [PubMed: 29051379]

Bankevich A, Nurk S, Antipov D, Gurevich AA, Dvorkin M, Kulikov AS, Lesin VM, Nikolenko SI, Pham S, Prjibelski AD, et al. (2012). SPAdes: a new genome assembly algorithm and its applications to single-cell sequencing. J. Comput. Biol 19, 455–477. [PubMed: 22506599]

Beklen A, Ainola M, Hukkanen M, Gürgan C, Sorsa T, and Konttinen YT (2007). MMPs, IL-1, and TNF are regulated by IL-17 in periodontitis. J. Dent. Res 86, 347–351. [PubMed: 17384030]

Bloom SM, Bijanki VN, Nava GM, Sun L, Malvin NP, Donermeyer DL, Dunne WM Jr., Allen PM, and Stappenbeck TS (2011). Commensal Bacteroides species induce colitis in host-genotype-specific fashion in a mouse model of inflammatory bowel disease. Cell Host Microbe 9, 390–403. [PubMed: 21575910]

Brandtzaeg P (2001). Inflammatory bowel disease: clinics and pathology. Do inflammatory bowel disease and periodontal disease have similar immunopathogeneses? Acta Odontol. Scand 59, 235–243. [PubMed: 11570527]

Briskin M, Winsor-Hines D, Shyjan A, Cochran N, Bloom S, Wilson J, McEvoy LM, Butcher EC, Kassam N, Mackay CR, et al. (1997). Human mucosal addressin cell adhesion molecule−1 is preferentially expressed in intestinal tract and associated lymphoid tissue. Am. J. Pathol 151, 97–110. [PubMed: 9212736]

Brito F, de Barros FC, Zaltman C, Carvalho AT, Carneiro AJ, Fischer RG, Gustafsson A, and Figueredo CM (2008). Prevalence of periodontitis and DMFT index in patients with Crohn's disease and ulcerative colitis. J. Clin. Periodontol 35, 555–560. [PubMed: 18400026]

Burr MD, Clark SJ, Spear CR, and Camper AK (2006). Denaturing gradient gel electrophoresis can rapidly display the bacterial diversity contained in 16S rDNA clone libraries. Microb. Ecol 51, 479–486. [PubMed: 16645925]

Calderón-Gómez E, Bassolas-Molina H, Mora-Buch R, Dotti I, Planell N, Esteller M, Gallego M, Martí M, Garcia-Martín C, Martínez-Torró C, et al. (2016). Commensal-Specific CD4(+) Cells From Patients With Crohn's Disease Have a T-Helper 17 Inflammatory Profile. Gastroenterology 151, 489–500.e3. [PubMed: 27267052]

Chen GY, Liu M, Wang F, Bertin J, and Núñez G (2011). A functional role for Nlrp6 in intestinal inflammation and tumorigenesis. J. Immunol 186, 7187–7194. [PubMed: 21543645]

Cheng WC, van Asten SD, Burns LA, Evans HG, Walter GJ, Hashim A, Hughes FJ, and Taams LS (2016). Periodontitis-associated pathogens P. gingivalis and A. actinomycetemcomitans activate human CD14(+) monocytes leading to enhanced Th17/IL-17 responses. Eur. J. Immunol 46, 2211–2221. [PubMed: 27334899]

Cooper HS, Murthy SN, Shah RS, and Sedergran DJ (1993). Clinicopathologic study of dextran sulfate sodium experimental murine colitis. Lab. Invest 69, 238–249. [PubMed: 8350599]

Curtis MM, Hu Z, Klimko C, Narayanan S, Deberardinis R, and Sperandio V (2014). The gut commensal Bacteroides thetaiotaomicron exacerbates enteric infection through modification of the metabolic landscape. Cell Host Microbe 16, 759–769. [PubMed: 25498343]

Dutzan N, Kajikawa T, Abusleme L, Greenwell-Wild T, Zuazo CE, Ikeuchi T, Brenchley L, Abe T, Hurabielle C, Martin D, et al. (2018). A dysbiotic microbiome triggers TH17 cells to mediate oral mucosal immunopathology in mice and humans. Sci. Transl. Med 10, eaat0797. [PubMed: 30333238]

Elinav E, Strowig T, Kau AL, Henao-Mejia J, Thaiss CA, Booth CJ, Peaper DR, Bertin J, Eisenbarth SC, Gordon JI, and Flavell RA (2011). NLRP6 inflammasome regulates colonic microbial ecology and risk for colitis. Cell 145, 745–757. [PubMed: 21565393]

Ellett JD, Evans ZP, Atkinson C, Schmidt MG, Schnellmann RG, and Chavin KD (2009). Toll-like receptor 4 is a key mediator of murine steatotic liver warm ischemia/reperfusion injury. Liver Transpl 15, 1101–1109. [PubMed: 19718644]

Erben U, Loddenkemper C, Doerfel K, Spieckermann S, Haller D, Heimesaat MM, Zeitz M, Siegmund B, and Kühl AA (2014). A guide to histomorphological evaluation of intestinal inflammation in mouse models. Int. J. Clin. Exp. Pathol 7, 4557–4576. [PubMed: 25197329]

Eskan MA, Jotwani R, Abe T, Chmelar J, Lim JH, Liang S, Ciero PA, Krauss JL, Li F, Rauner M, et al. (2012). The leukocyte integrin antagonist Del−1 inhibits IL-17-mediated inflammatory bone loss. Nat. Immunol 13, 465–473. [PubMed: 22447028]

Faith JJ, Ahern PP, Ridaura VK, Cheng J, and Gordon JI (2014). Identifying gut microbe-host phenotype relationships using combinatorial communities in gnotobiotic mice. Sci. Transl. Med 6, 220ra11.

Franchi L, Amer A, Body-Malapel M, Kanneganti TD, Ozören N, Jagirdar R, Inohara N, Vandenabeele P, Bertin J, Coyle A, et al. (2006). Cytosolic flagellin requires Ipaf for activation of caspase−1 and interleukin 1beta in salmonella-infected macrophages. Nat. Immunol 7, 576–582. [PubMed: 16648852]

Franchi L, Kamada N, Nakamura Y, Burberry A, Kuffa P, Suzuki S, Shaw MH, Kim YG, and Núñez G (2012). NLRC4-driven production of IL-1β discriminates between pathogenic and commensal bacteria and promotes host intestinal defense. Nat. Immunol 13, 449–456. [PubMed: 22484733]

Furusawa Y, Obata Y, Fukuda S, Endo TA, Nakato G, Takahashi D, Nakanishi Y, Uetake C, Kato K, Kato T, et al. (2013). Commensal microbe-derived butyrate induces the differentiation of colonic regulatory T cells. Nature 504, 446–450. [PubMed: 24226770]

Garrett WS (2015). Cancer and the microbiota. Science 348, 80–86. [PubMed: 25838377]

Gevers D, Kugathasan S, Denson LA, Vázquez-Baeza Y, Van Treuren W, Ren B, Schwager E, Knights D, Song SJ, Yassour M, et al. (2014). The treatment-naive microbiome in new-onset Crohn's disease. Cell Host Microbe 15, 382–392. [PubMed: 24629344]

Haberman Y, Tickle TL, Dexheimer PJ, Kim MO, Tang D, Karns R, Baldassano RN, Noe JD, Rosh J, Markowitz J, et al. (2014). Pediatric Crohn disease patients exhibit specific ileal transcriptome and microbiome signature. J. Clin. Invest 124, 3617–3633. [PubMed: 25003194]

Harbour SN, Maynard CL, Zindl CL, Schoeb TR, and Weaver CT (2015). Th17 cells give rise to Th1 cells that are required for the pathogenesis of colitis. Proc. Natl. Acad. Sci. USA 112, 7061–7066. [PubMed: 26038559]

He Y, Zeng MY, Yang D, Motro B, and Núñez G (2016). NEK7 is an essential mediator of NLRP3 activation downstream of potassium efflux. Nature 530, 354–357. [PubMed: 26814970]

Hecht G, Bar-Nathan C, Milite G, Alon I, Moshe Y, Greenfeld L, Dotsenko N, Suez J, Levy M, Thaiss CA, et al. (2014). A simple cage-autonomous method for the maintenance of the barrier status of germ-free mice during experimentation. Lab. Anim 48, 292–297. [PubMed: 25097255]

Hegazy AN, West NR, Stubbington MJT, Wendt E, Suijker KIM, Datsi A, This S, Danne C, Campion S, Duncan SH, et al.; Oxford IBD Cohort Investigators (2017). Circulating and Tissue-Resident $CD4^+$ T Cells With Reactivity to Intestinal Microbiota Are Abundant in Healthy Individuals and Function Is Altered During Inflammation. Gastroenterology 153, 1320–1337.e16. [PubMed: 28782508]

Hepworth MR, Fung TC, Masur SH, Kelsen JR, McConnell FM, Dubrot J, Withers DR, Hugues S, Farrar MA, Reith W, et al. (2015). Immune tolerance. Group 3 innate lymphoid cells mediate

intestinal selection of commensal bacteria-specific CD4$^+$ T cells. Science 348, 1031–1035. [PubMed: 25908663]

Imhann F, Bonder MJ, Vich Vila A, Fu J, Mujagic Z, Vork L, Tigchelaar EF, Jankipersadsing SA, Cenit MC, Harmsen HJ, et al. (2016). Proton pump inhibitors affect the gut microbiome. Gut 65, 740–748. [PubMed: 26657899]

Irrazábal T, Belcheva A, Girardin SE, Martin A, and Philpott DJ (2014). The multifaceted role of the intestinal microbiota in colon cancer. Mol. Cell 54, 309–320. [PubMed: 24766895]

Ivanov II, Atarashi K, Manel N, Brodie EL, Shima T, Karaoz U, Wei D, Goldfarb KC, Santee CA, Lynch SV, et al. (2009). Induction of intestinal Th17 cells by segmented filamentous bacteria. Cell 139, 485–498. [PubMed: 19836068]

Jackson MA, Goodrich JK, Maxan ME, Freedberg DE, Abrams JA, Poole AC, Sutter JL, Welter D, Ley RE, Bell JT, et al. (2016). Proton pump inhibitors alter the composition of the gut microbiota. Gut 65, 749–756. [PubMed: 26719299]

Jiao Y, Darzi Y, Tawaratsumida K, Marchesan JT, Hasegawa M, Moon H, Chen GY, Núñez G, Giannobile WV, Raes J, and Inohara N (2013). Induction of bone loss by pathobiont-mediated Nod1 signaling in the oral cavity. Cell Host Microbe 13, 595–601. [PubMed: 23684310]

Johansson-Lindbom B, Svensson M, Pabst O, Palmqvist C, Marquez G, Förster R, and Agace WW (2005). Functional specialization of gut CD103+ dendritic cells in the regulation of tissue-selective T cell homing. J. Exp. Med 202, 1063–1073. [PubMed: 16216890]

Juillerat P, Schneeweiss S, Cook EF, Ananthakrishnan AN, Mogun H, and Korzenik JR (2012). Drugs that inhibit gastric acid secretion may alter the course of inflammatory bowel disease. Aliment. Pharmacol. Ther 36, 239–247. [PubMed: 22670722]

Kilkenny C, Browne WJ, Cuthill IC, Emerson M, and Altman DG (2010). Improving bioscience research reporting: the ARRIVE guidelines for reporting animal research. PLoS Biol. 8, e1000412. [PubMed: 20613859]

Kitamoto S, Alteri CJ, Rodrigues M, Nagao-Kitamoto H, Sugihara K, Himpsl SD, Bazzi M, Miyoshi M, Nishioka T, Hayashi A, et al. (2020). Dietary L-serine confers a competitive fitness advantage to Enterobacteriaceae in the inflamed gut. Nat. Microbiol 5, 116–125. [PubMed: 31686025]

Klopfleisch R (2013). Multiparametric and semiquantitative scoring systems for the evaluation of mouse model histopathology–a systematic review. BMC Vet. Res 9, 123. [PubMed: 23800279]

Knodler LA, Crowley SM, Sham HP, Yang H, Wrande M, Ma C, Ernst RK, Steele-Mortimer O, Celli J, and Vallance BA (2014). Noncanonical inflammasome activation of caspase−4/caspase−11 mediates epithelial defenses against enteric bacterial pathogens. Cell Host Microbe 16, 249–256. [PubMed: 25121752]

Lankarani KB, Sivandzadeh GR, and Hassanpour S (2013). Oral manifestation in inflammatory bowel disease: a review. World J. Gastroenterol 19, 8571–8579. [PubMed: 24379574]

Liu L, Dong Y, Ye M, Jin S, Yang J, Joosse ME, Sun Y, Zhang J, Lazarev M, Brant SR, et al. (2017). The Pathogenic Role of NLRP3 Inflammasome Activation in Inflammatory Bowel Diseases of Both Mice and Humans. J. Crohn's Colitis 11, 737–750. [PubMed: 27993998]

Lourenço SV, Hussein TP, Bologna SB, Sipahi AM, and Nico MM (2010). Oral manifestations of inflammatory bowel disease: a review based on the observation of six cases. J. Eur. Acad. Dermatol. Venereol 24, 204–207. [PubMed: 19552719]

Lu XL, Zhao CH, Zhang H, and Yao XL (2017). iRhom2 is involved in lipopolysaccharide-induced cardiac injury in vivo and in vitro through regulating inflammation response. Biomed. Pharmacother 86, 645–653. [PubMed: 28033581]

Man SM, Karki R, Briard B, Burton A, Gingras S, Pelletier S, and Kanneganti TD (2017). Differential roles of caspase−1 and caspase−11 in infection and inflammation. Sci. Rep 7, 45126. [PubMed: 28345580]

Marchesan J, Girnary MS, Jing L, Miao MZ, Zhang S, Sun L, Morelli T, Schoenfisch MH, Inohara N, Offenbacher S, and Jiao Y (2018). An experimental murine model to study periodontitis. Nat. Protoc 13, 2247–2267. [PubMed: 30218100]

Miyata H, Castaneda JM, Fujihara Y, Yu Z, Archambeault DR, Isotani A, Kiyozumi D, Kriseman ML, Mashiko D, Matsumura T, et al. (2016). Genome engineering uncovers 54 evolutionarily

conserved and testis-enriched genes that are not required for male fertility in mice. Proc. Natl. Acad. Sci. USA 113, 7704–7710. [PubMed: 27357688]

Mora JR, Bono MR, Manjunath N, Weninger W, Cavanagh LL, Rosemblatt M, and Von Andrian UH (2003). Selective imprinting of gut-homing T cells by Peyer's patch dendritic cells. Nature 424, 88–93. [PubMed: 12840763]

Morton AM, Sefik E, Upadhyay R, Weissleder R, Benoist C, and Mathis D (2014). Endoscopic photoconversion reveals unexpectedly broad leukocyte trafficking to and from the gut. Proc. Natl. Acad. Sci. USA 111, 6696–6701. [PubMed: 24753589]

Moutsopoulos NM, Konkel J, Sarmadi M, Eskan MA, Wild T, Dutzan N, Abusleme L, Zenobia C, Hosur KB, Abe T, et al. (2014). Defective neutrophil recruitment in leukocyte adhesion deficiency type I disease causes local IL-17-driven inflammatory bone loss. Sci. Transl. Med 6, 229ra40.

Murthy SN, Cooper HS, Shim H, Shah RS, Ibrahim SA, and Sedergran DJ (1993). Treatment of dextran sulfate sodium-induced murine colitis by intracolonic cyclosporin. Dig. Dis. Sci 38, 1722–1734. [PubMed: 8359087]

Nagao-Kitamoto H, Shreiner AB, Gillilland MG 3rd, Kitamoto S, Ishii C, Hirayama A, Kuffa P, El-Zaatari M, Grasberger H, Seekatz AM, et al. (2016). Functional characterization of inflammatory bowel disease-associated gut dysbiosis in gnotobiotic mice. Cell. Mol. Gastroenterol. Hepatol 2, 468–481. [PubMed: 27795980]

Neurath MF (2014). New targets for mucosal healing and therapy in inflammatory bowel diseases. Mucosal Immunol. 7, 6–19. [PubMed: 24084775]

Okumura R, Kurakawa T, Nakano T, Kayama H, Kinoshita M, Motooka D, Gotoh K, Kimura T, Kamiyama N, Kusu T, et al. (2016). Lypd8 promotes the segregation of flagellated microbiota and colonic epithelia. Nature 532, 117–121. [PubMed: 27027293]

Ono Y, Kanai T, Sujino T, Nemoto Y, Kanai Y, Mikami Y, Hayashi A, Matsumoto A, Takaishi H, Ogata H, et al. (2012). T-helper 17 and interleukin−17-producing lymphoid tissue inducer-like cells make different contributions to colitis in mice. Gastroenterology 143, 1288–1297. [PubMed: 22850180]

Paik J, Pershutkina O, Meeker S, Yi JJ, Dowling S, Hsu C, Hajjar AM, Maggio-Price L, and Beck DA (2015). Potential for using a hermeticallysealed, positive-pressured isocage system for studies involving germ-free mice outside a flexible-film isolator. Gut Microbes 6, 255–265. [PubMed: 26177210]

Pakala SB, Reddy SD, Bui-Nguyen TM, Rangparia SS, Bommana A, and Kumar R (2010). MTA1 coregulator regulates LPS response via MyD88-dependent signaling. J. Biol. Chem 285, 32787–32792. [PubMed: 20702415]

Park E, Na HS, Song YR, Shin SY, Kim YM, and Chung J (2014). Activation of NLRP3 and AIM2 inflammasomes by Porphyromonas gingivalis infection. Infect. Immun 82, 112–123. [PubMed: 24126516]

Pietropaoli D, Del Pinto R, Corridoni D, Rodriguez-Palacios A, Di Stefano G, Monaco A, Weinberg A, and Cominelli F (2014). Occurrence of spontaneous periodontal disease in the SAMP1/YitFc murine model of Crohn disease. J. Periodontol 85, 1799–1805. [PubMed: 25019175]

Rathinam VA, Vanaja SK, Waggoner L, Sokolovska A, Becker C, Stuart LM, Leong JM, and Fitzgerald KA (2012). TRIF licenses caspase−11-dependent NLRP3 inflammasome activation by gram-negative bacteria. Cell 150, 606–619. [PubMed: 22819539]

Reed M, Luissint AC, Azcutia V, Fan S, O'Leary MN, Quiros M, Brazil J, Nusrat A, and Parkos CA (2019). Epithelial CD47 is critical for mucosal repair in the murine intestine in vivo. Nat. Commun 10, 5004. [PubMed: 31676794]

Round JL, Lee SM, Li J, Tran G, Jabri B, Chatila TA, and Mazmanian SK (2011). The Toll-like receptor 2 pathway establishes colonization by a commensal of the human microbiota. Science 332, 974–977. [PubMed: 21512004]

Said HS, Suda W, Nakagome S, Chinen H, Oshima K, Kim S, Kimura R, Iraha A, Ishida H, Fujita J, et al. (2014). Dysbiosis of salivary microbiota in inflammatory bowel disease and its association with oral immunological biomarkers. DNA Res. 21, 15–25. [PubMed: 24013298]

Sand J, Haertel E, Biedermann T, Contassot E, Reichmann E, French LE, Werner S, and Beer HD (2018). Expression of inflammasome proteins and inflammasome activation occurs in human, but not in murine keratinocytes. Cell Death Dis. 9, 24. [PubMed: 29348630]

Sato T, Vries RG, Snippert HJ, van de Wetering M, Barker N, Stange DE, van Es JH, Abo A, Kujala P, Peters PJ, and Clevers H (2009). Single Lgr5 stem cells build crypt-villus structures in vitro without a mesenchymal niche. Nature 459, 262–265. [PubMed: 19329995]

Schirmer M, Denson L, Vlamakis H, Franzosa EA, Thomas S, Gotman NM, Rufo P, Baker SS, Sauer C, Markowitz J, et al. (2018). Compositional and Temporal Changes in the Gut Microbiome of Pediatric Ulcerative Colitis Patients Are Linked to Disease Course. Cell Host Microbe 24, 600–610.e4. [PubMed: 30308161]

Schloss PD, Westcott SL, Ryabin T, Hall JR, Hartmann M, Hollister EB, Lesniewski RA, Oakley BB, Parks DH, Robinson CJ, et al. (2009). Introducing mothur: open-source, platform-independent, community-supported software for describing and comparing microbial communities. Appl. Environ. Microbiol 75, 7537–7541. [PubMed: 19801464]

Schmidt TS, Hayward MR, Coelho LP, Li SS, Costea PI, Voigt AY, Wirbel J, Maistrenko OM, Alves RJ, Bergsten E, et al. (2019). Extensive transmission of microbes along the gastrointestinal tract. eLife 8, e42693. [PubMed: 30747106]

Seemann T (2014). Prokka: rapid prokaryotic genome annotation. Bioinformatics 30, 2068–2069. [PubMed: 24642063]

Segata N, Izard J, Waldron L, Gevers D, Miropolsky L, Garrett WS, and Huttenhower C (2011). Metagenomic biomarker discovery and explanation. Genome Biol. 12, R60. [PubMed: 21702898]

Seo SU, Kamada N, Muñoz-Planillo R, Kim YG, Kim D, Koizumi Y, Hasegawa M, Himpsl SD, Browne HP, Lawley TD, et al. (2015). Distinct Commensals Induce Interleukin−1β via NLRP3 Inflammasome in Inflammatory Monocytes to Promote Intestinal Inflammation in Response to Injury. Immunity 42, 744–755. [PubMed: 25862092]

Seregin SS, Golovchenko N, Schaf B, Chen J, Pudlo NA, Mitchell J, Baxter NT, Zhao L, Schloss PD, Martens EC, et al. (2017). NLRP6 Protects $Il10^{-/-}$ Mice from Colitis by Limiting Colonization of Akkermansia muciniphila. Cell Rep. 19, 733–745. [PubMed: 28445725]

Shah R, Richardson P, Yu H, Kramer J, and Hou JK (2017). Gastric Acid Suppression Is Associated with an Increased Risk of Adverse Outcomes in Inflammatory Bowel Disease. Digestion 95, 188–193. [PubMed: 28288458]

Shaw MH, Kamada N, Kim YG, and Núñez G (2012). Microbiota-induced IL-1β, but not IL−6, is critical for the development of steady-state TH17 cells in the intestine. J. Exp. Med 209, 251–258. [PubMed: 22291094]

Shen C, Landers CJ, Derkowski C, Elson CO, and Targan SR (2008). Enhanced CBir1-specific innate and adaptive immune responses in Crohn's disease. Inflamm. Bowel Dis 14, 1641–1651. [PubMed: 18825772]

Singh N, Gurav A, Sivaprakasam S, Brady E, Padia R, Shi H, Thangaraju M, Prasad PD, Manicassamy S, Munn DH, et al. (2014). Activation of Gpr109a, receptor for niacin and the commensal metabolite butyrate, suppresses colonic inflammation and carcinogenesis. Immunity 40, 128–139. [PubMed: 24412617]

Takahashi K, Azuma T, Motohira H, Kinane DF, and Kitetsu S (2005). The potential role of interleukin −17 in the immunopathology of periodontal disease. J. Clin. Periodontol 32, 369–374. [PubMed: 15811054]

Tomura M, Yoshida N, Tanaka J, Karasawa S, Miwa Y, Miyawaki A, and Kanagawa O (2008). Monitoring cellular movement in vivo with photoconvertible fluorescence protein "Kaede" transgenic mice. Proc. Natl. Acad. Sci. USA 105, 10871–10876. [PubMed: 18663225]

Van Dyke TE, Dowell VR Jr., Offenbacher S, Snyder W, and Hersh T (1986). Potential role of microorganisms isolated from periodontal lesions in the pathogenesis of inflammatory bowel disease. Infect. Immun 53, 671–677. [PubMed: 3462153]

Vavricka SR, Manser CN, Hediger S, Vögelin M, Scharl M, Biedermann L, Rogler S, Seibold F, Sanderink R, Attin T, et al. (2013). Periodontitis and gingivitis in inflammatory bowel disease: a case-control study. Inflamm. Bowel Dis 19, 2768–2777. [PubMed: 24216685]

Wang X, Gong P, Zhang X, Wang J, Tai L, Wang X, Wei Z, Yang Y, Yang Z, Li J, and Zhang X (2017). NLRP3 inflammasome activation in murine macrophages caused by Neospora caninum infection. Parasit. Vectors 10, 266. [PubMed: 28558839]

Watanabe T, Tanaka G, Hamada S, Namiki C, Suzuki T, Nakajima M, and Furihata C (2009). Dose-dependent alterations in gene expression in mouse liver induced by diethylnitrosamine and ethylnitrosourea and determined by quantitative real-time PCR. Mutat. Res 673, 9–20. [PubMed: 19100860]

Winter SE, Winter MG, Xavier MN, Thiennimitr P, Poon V, Keestra AM, Laughlin RC, Gomez G, Wu J, Lawhon SD, et al. (2013). Host-derived nitrate boosts growth of E. coli in the inflamed gut. Science 339, 708–711. [PubMed: 23393266]

Xu M, Pokrovskii M, Ding Y, Yi R, Au C, Harrison OJ, Galan C, Belkaid Y, Bonneau R, and Littman DR (2018). c-MAF-dependent regulatory T cells mediate immunological tolerance to a gut pathobiont. Nature 554, 373–377. [PubMed: 29414937]

Zhu W, Winter MG, Byndloss MX, Spiga L, Duerkop BA, Hughes ER, Büttner L, de Lima Romão E, Behrendt CL, Lopez CA, et al. (2018). Precision editing of the gut microbiota ameliorates colitis. Nature 553, 208–211. [PubMed: 29323293]

Highlights

- Oral inflammation triggers expansion of oral pathobionts
- Ectopic gut colonization by oral pathobionts promotes colitis through IL-1β
- Oral Th17 cells that arise during oral inflammation can migrate to the gut
- Oral pathobiont-reactive Th17 cells that migrate to the gut contribute to colitis

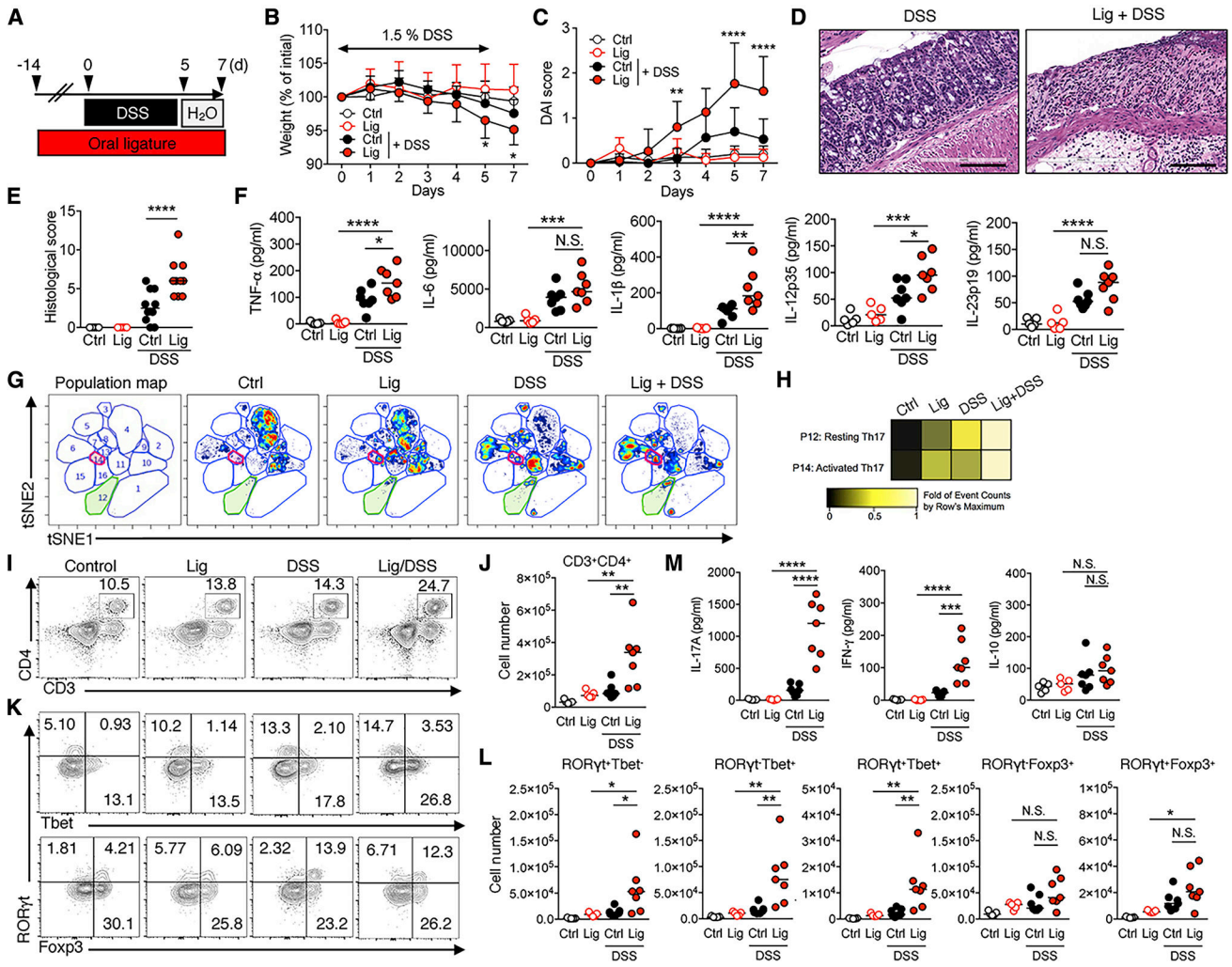

Figure 1. Periodontitis Exacerbates Intestinal Inflammation

(A) SPF C57BL/6 mice received oral ligatures. At day 14, 1.5% DSS was given for 5 days, followed by regular water for 2 days. Mice were sacrificed at day 7 after DSS treatment.

(B and C) Body weight and disease activity index (DAI). (−) DSS group, N = 5; (+) DSS group, N = 10.

(D) Representative colonic histological images (scale bar, 100 μm).

(E) Colonic histological score evaluated by the criteria for the DSS-induced colitis model.

(F) Isolated colonic *lamina propria* (LP) cells were cultured (24 h), and secreted cytokines production was measured by ELISA.

(G) cLP cells (pooled from 5 individual mice) were analyzed by CyTOF. A viSNE analysis was performed to identify main population differences among the four treatment groups. Each cluster is identified by its marker expression profile (Table S1). Density plots for the population clusters are shown.

(H) Heatmap (populations 12 and 14) showing calculated fold of event counts by Row's maximum using the x axis channel.

(I and J) Representative flow cytometry plots and numbers of $CD3^{+}CD4^{+}$ T cells in the cLP.

(K and L) Representative flow cytometry plots and numbers of Th1, Th17, and Treg cells in the cLP.

(M) Cytokine production from $CD4^+$ LP cells re-stimulated with αCD3/28 Abs for 24 h. Results are shown as mean ± SD (two-way ANOVA) or median (one-way ANOVA). Each dot indicates an individual mouse (N = 5–10). N.S., not significant; *p < 0.05, **p < 0.01, ***p < 0.001, ****p < 0.0001 by two-way ANOVA followed by Bonferroni post hoc test (B and C) or one-way ANOVA followed by Bonferroni post hoc test (E, F, J, L, and M). See also Figures S1 and S2 and Table S1.

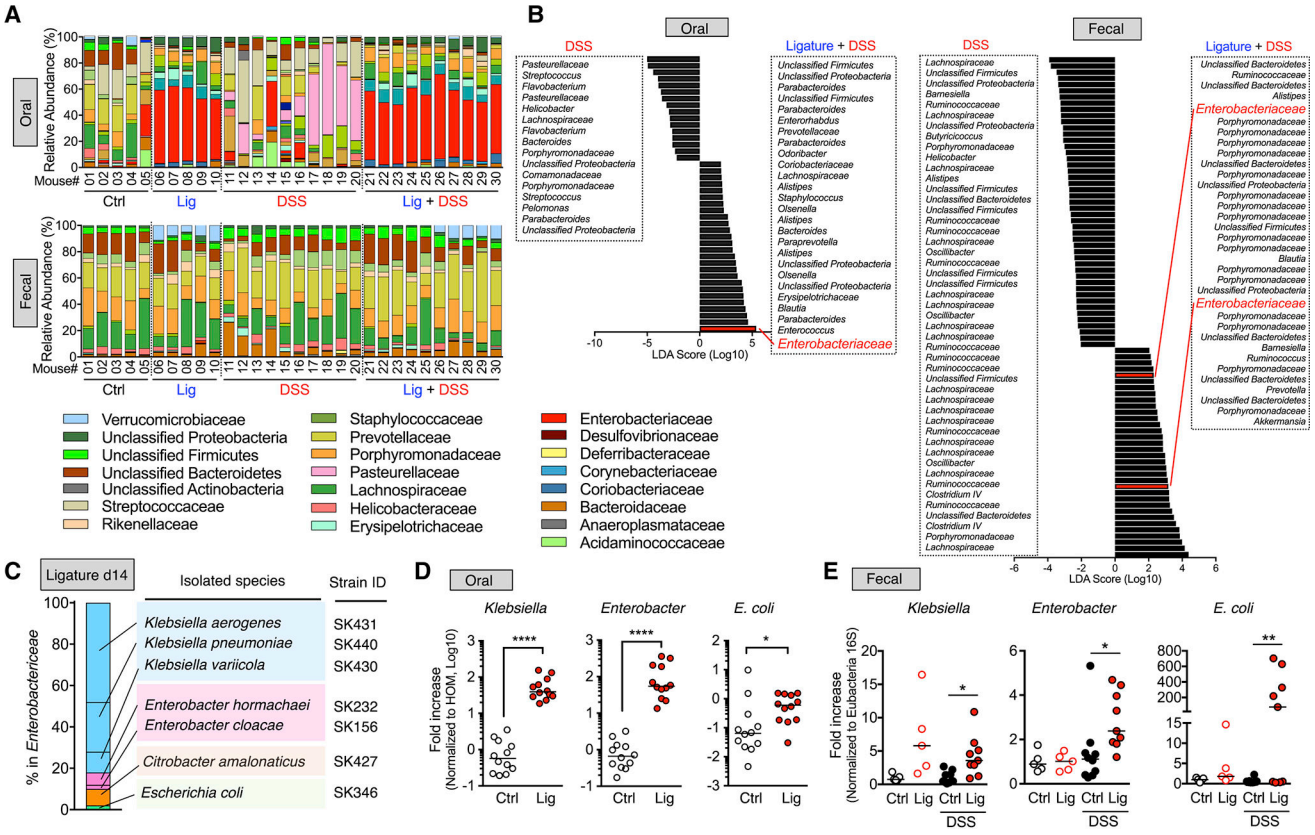

Figure 2. Enterobacteriaceae Accumulate in Both the Oral Cavity and the Gut of Periodontitis-Colitis Mice

(A) Periodontitis was induced in SPF C57BL/6 mice by insertion of oral ligatures. Microbial changes in the oral cavity and fecal contents were analyzed by 16S rRNA sequencing.

(B) Commonly enriched bacterial families in the oral cavity and gut in ligature-DSS mice compared with DSS mice were analyzed by LEfSe.

(C–E) *Enterobacteriaceae* species isolated from oral cavities of dysbiotic mice (day 14 ligature). The abundance of the indicated bacterial species in the oral cavity (D) and feces (E) was assessed by qPCR. The abundance of bacteria relative to that found in non-ligatured control (Ctrl) mice is shown. Each dot indicates an individual mouse (N = 5–12). *p < 0.05, **p < 0.01, ****p < 0.0001 by Mann–Whitney *U* test (D) or by one-way ANOVA followed by Bonferroni post hoc test (E).

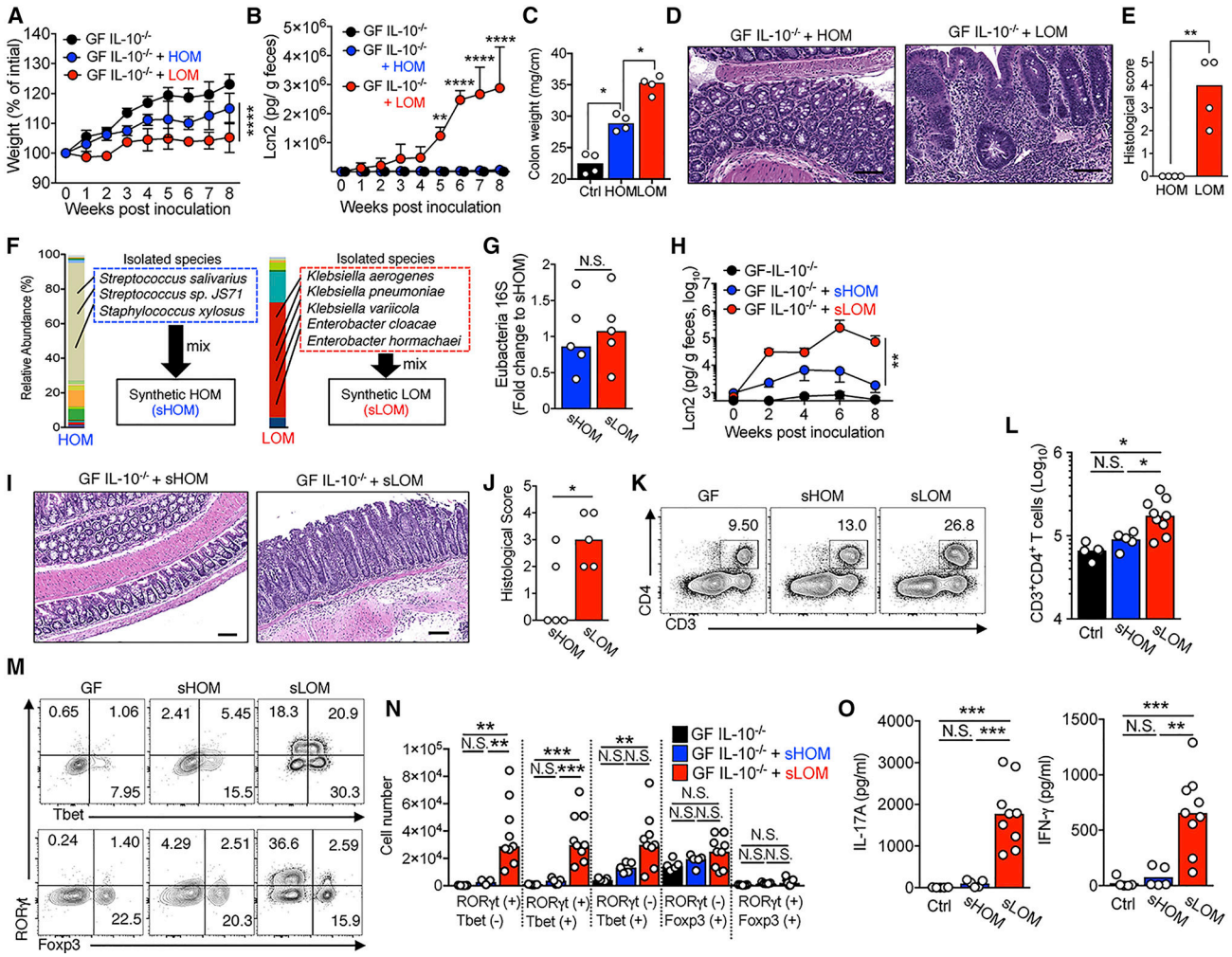

Figure 3. Ectopic Gut Colonization by Oral Pathobionts Leads to Development of Colitis in Genetically Susceptible Hosts

(A–E) Oral microbiota from healthy (3-h ligature placement, healthy oral microbiota [HOM]) and periodontitis (14-day ligature placement, ligature-associated microbiota [LOM]) mice were harvested. *Il10*$^{-/-}$ gnotobiotic mice were colonized with HOM or LOM and maintained for 56 days.

(A and B) Body weight and fecal Lcn2 levels were monitored weekly.

(C) Colon weight on day 56.

(D and E) Representative colonic histological images (scale bar, 100 μm) and score (day 56) assessed by the criteria for the *Il10*$^{-/-}$ colitis model.

(F–O) Synthetic microbial communities that mimic HOM and LOM were generated by combining bacterial isolates from the most abundant families that consist of oral microbes normally associated with oral health (synthetic HOM [sHOM]) or oral microbes associated with oral dysbiosis (synthetic LOM [sLOM]). Synthetic communities were inoculated into *Il10*$^{-/-}$ mice as described in (A)–(E).

(G) Total bacteria burden (Eubacteria 16S rRNA) in feces from each group was quantified by qPCR (normalized to fecal weight).

(H) Fecal Lcn2 levels.

(I and J) Representative colonic histological images (scale bar, 100 μm) and histological score on day 56, assessed by the criteria for the *Il10*$^{-/-}$ colitis model.
(K and L) Representative flow cytometry plots and number of CD3^{+}CD4^{+} T cells in the cLP.
(M and N) Representative flow cytometry plots and numbers of Th1, Th17, and Treg cells in the cLP.
(O) Cytokine production from CD4^{+} LP cells re-stimulated with αCD3/28 Abs for 24 h.
Results are shown as mean ± SD (two-way ANOVA) or median (one-way ANOVA). Each dot indicates an individual mouse (N = 5–9). *p < 0.05, **p < 0.01, ***p < 0.001, ****p < 0.0001 by two-way ANOVA followed by Bonferroni post hoc test (A, B, and H), one-way ANOVA followed by Bonferroni post hoc test (C, L, N, and O), or Mann-Whitney *U* test (E, G, and J).

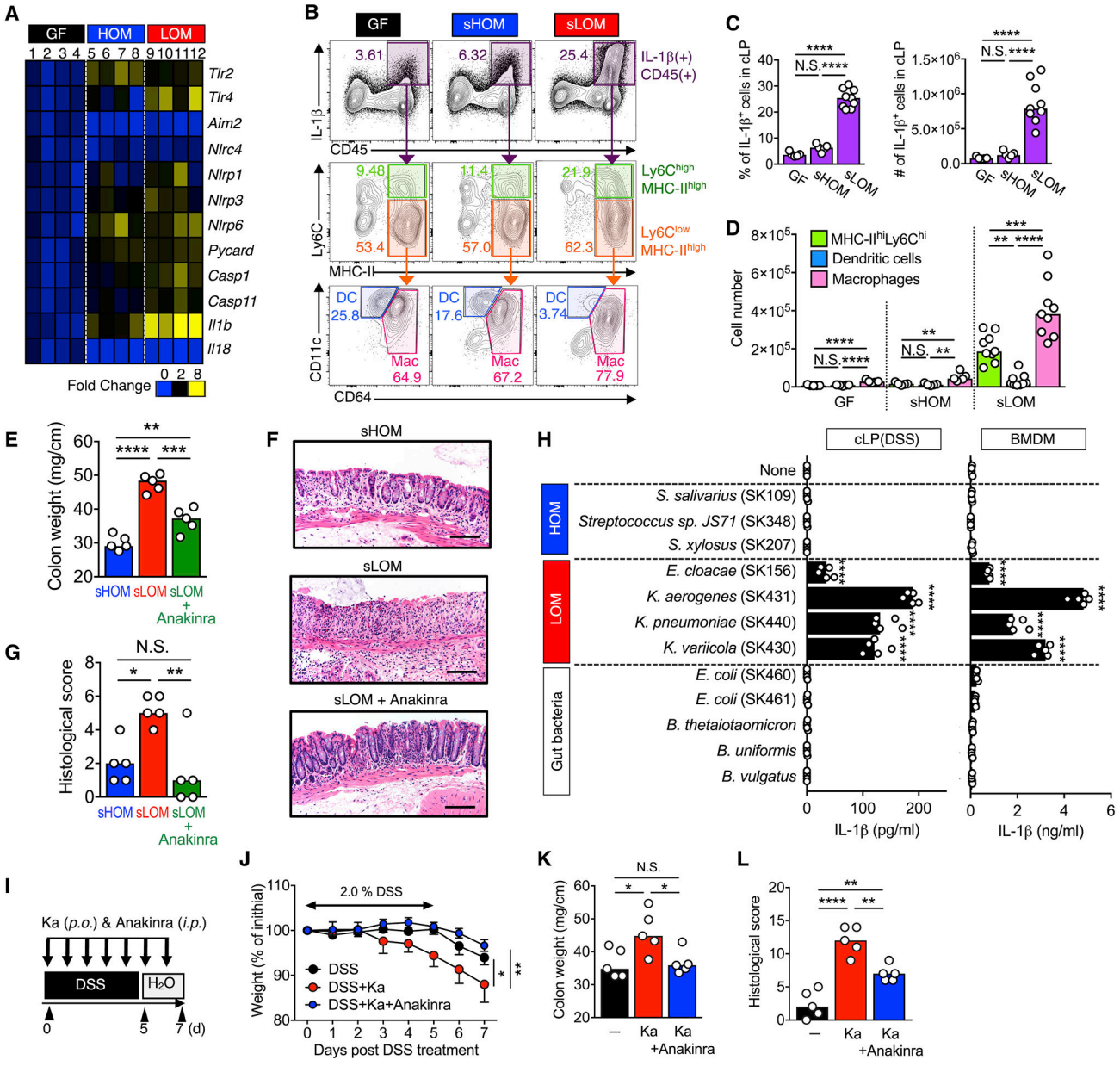

Figure 4. Oral Pathobionts Elicit Colitis via Activation of the Inflammasome

(A) Heatmap showing fold mRNA increase (qPCR) of the indicated genes in colonic tissues of each group (Ctrl orHOM- or LOM-colonized *Il10*$^{-/-}$ gnotobiotic mice shown in Figures 3A–3E).

(B) Gating strategy showing IL-1β^{+} leukocytes in the cLP of each group (Ctrl or sHOM- or sLOM-colonized *Il10*$^{-/-}$ gnotobiotic mice shown in Figures 3H–3L).

(C and D) Percentage of CD45+ IL-1β+ cells in cLP mononuclear cells (LPMCs) and numbers of MHC class IIhiLy6Chi dendritic cells (DCs) and macrophages (Mac).

(E) Gnotobiotic mice colonized by sham Ctrl (GF), sHOM, or sLOM at 7 days were treated with 1.5% DSS for 5 days in the absence or presence of anakinra (50 mg/kg/daily,

intraperitoneally [i.p.]), followed by an additional 2 days with regular water. Colon weight (milligrams per centimeter) after 7 days of DSS treatment is shown.

(F and G) Representative colonic histological images (scale bar, 100 μm) and histological score after 7 days of DSS treatment were evaluated by the criteria for the DSS colitis model.

(H) LPMCs (from mice treated with DSS) or bone marrow-derived Macs (BMDMs) were co-cultured with the indicated bacterial strains (MOI = 5) for 3 h. Gentamicin (100 μg/mL) was then added, and cells were cultured for an additional 16 h. IL-1β production in the supernatant was measured by ELISA.

(I) SPF B6 mice were treated with 2.0% DSS for 5 days, followed by an additional 2 days of regular water in the presence or absence of the oral pathobiont *K. aerogenes* (Ka; 109 colony-forming units [CFUs]/day, p.o.) and anakinra (50 mg/kg/day, i.p.).

(J) Kinetics of body weight change.

(K) Colon weight after 7 days of DSS treatment.

(L) Colonic histological score 7 days after DSS treatment, evaluated by the criteria for the DSS colitis model.

Results are shown as median (one-way ANOVA) or mean ± SD (two-way ANOVA). Each dot indicates an individual mouse (N = 5–9). *p < 0.05, **p < 0.01, ***p < 0.001, ****p < 0.0001 by one-way ANOVA followed by Bonferroni post hoc test (C–E, G, H, K, and L) or two-way ANOVA followed by Bonferroni post hoc test (J). See also Figures S3 and S4 and Table S2.

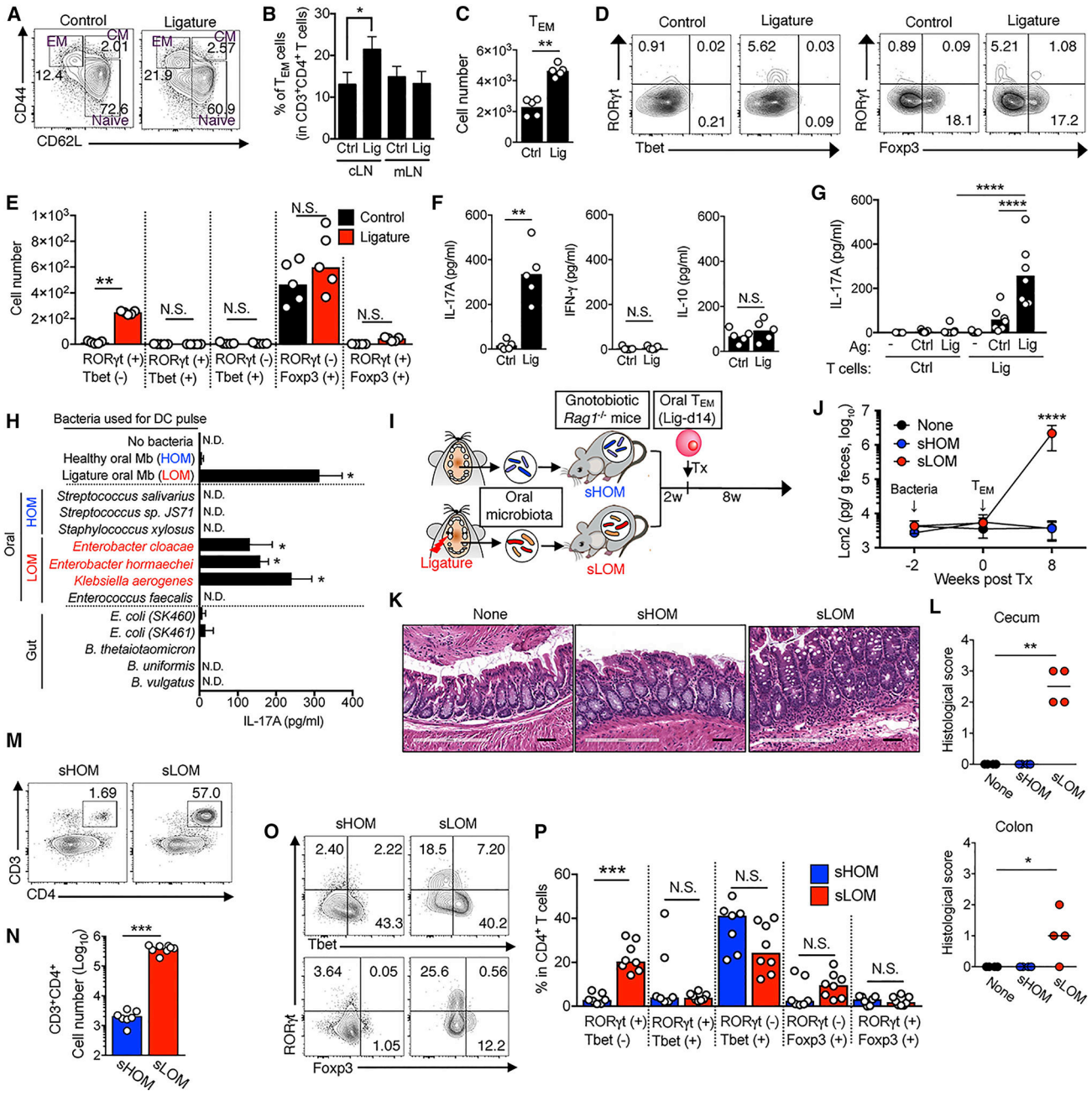

Figure 5. Periodontitis Elicits Generation of Oral Pathobiont-Reactive Th17 Cells

(A) Fluorescence-activated cell sorting (FACS) plot of $CD3^+CD4^+$ T cell subsets (naive ($CD3^+CD4^+CD44loCD62Lhi$), effector memory T (TEM) ($CD3^+CD4^+$ $CD44hiCD62Llo$), and central memory (CM) T ($CD3^+CD4^+CD44hiCD62Lhi$) cells in cLNs of Ctrl and ligatured (day 14) mice.

(B) Frequency of $CD3^+CD4^+$ TEM cells in cLNs and mesenteric LNs (mLN) in Ctrl and ligatured (day 14) mice.

(C) Number of TEM cells in cLN of mice with (day 14) or without ligatures.

(D and E) Representative flow cytometry plots and numbers of Th1, Th17, and Treg cells in cLNs.

(F) Cytokine production in supernatants from $CD3^+CD4^+$ T cells isolated from cLNs stimulated with αCD3/28 Abs for 24 h, measured by ELISA.

(G) Bone marrow-derived dendritic cells (BMDCs) were pulsed with heat-killed, freshly isolated HOM (3-h ligature) or LOM (14-day ligature). Pulsed BMDCs were washed and co-cultured with $CD3^+CD4^+$ T cells isolated from cLNs of Ctrl or ligature (day 14) mice for 24 h. Secreted IL-17A in supernatants was analyzed by ELISA.

(H) Responsiveness of oral $CD4^+$ memory T cells in ligature mice (day 14) to specific oral and gut commensal bacteria.

(I) GF *Rag1*$^{-/-}$ mice were colonized by sHOM or sLOM for 14 days. Oral $CD3^+CD4^+$CD44hiCD62LloCD25− TEM cells were isolated from the cLNs of ligature mice (day 14). Isolated TEM cells (2 × 105 cells/mouse) were then adoptively transferred into gnotobiotic (sHOM or sLOM) *Rag1*$^{-/-}$ mice and Ctrl GF *Rag1*$^{-/-}$ mice. Oral TEM cell-transferred *Rag1*$^{-/-}$ mice were maintained for 8 weeks.

(J) Fecal Lcn2 levels were monitored at the indicated time points.

(K and L) Representative histological images of a colon (scale bar, 100 μm) and histological score of a cecum and colon 8 weeks after oral TEM cell transfer, assessed by the criteria for the transfer colitis model.

(M and N) Representative flow cytometry plots and number of $CD3^+CD4^+$ T cells in the cLP.

(O and P) Representative flow cytometry plots and numbers of Th1, Th17, and Treg cells in the cLP.

Results are shown as mean ± SD (two-way ANOVA) or median (one-way ANOVA). Each dot indicates an individual mouse (N = 4–8). *$p < 0.05$, **$p < 0.01$, ***$p < 0.001$, ****$p < 0.0001$ by Mann-Whitney *U* test (B, C, E, F, N, and P), one-way ANOVA followed by Bonferroni post hoc test (G, L, and H), or two-way ANOVA followed by Bonferroni post hoc test (J). See also Figures S6 and S7.

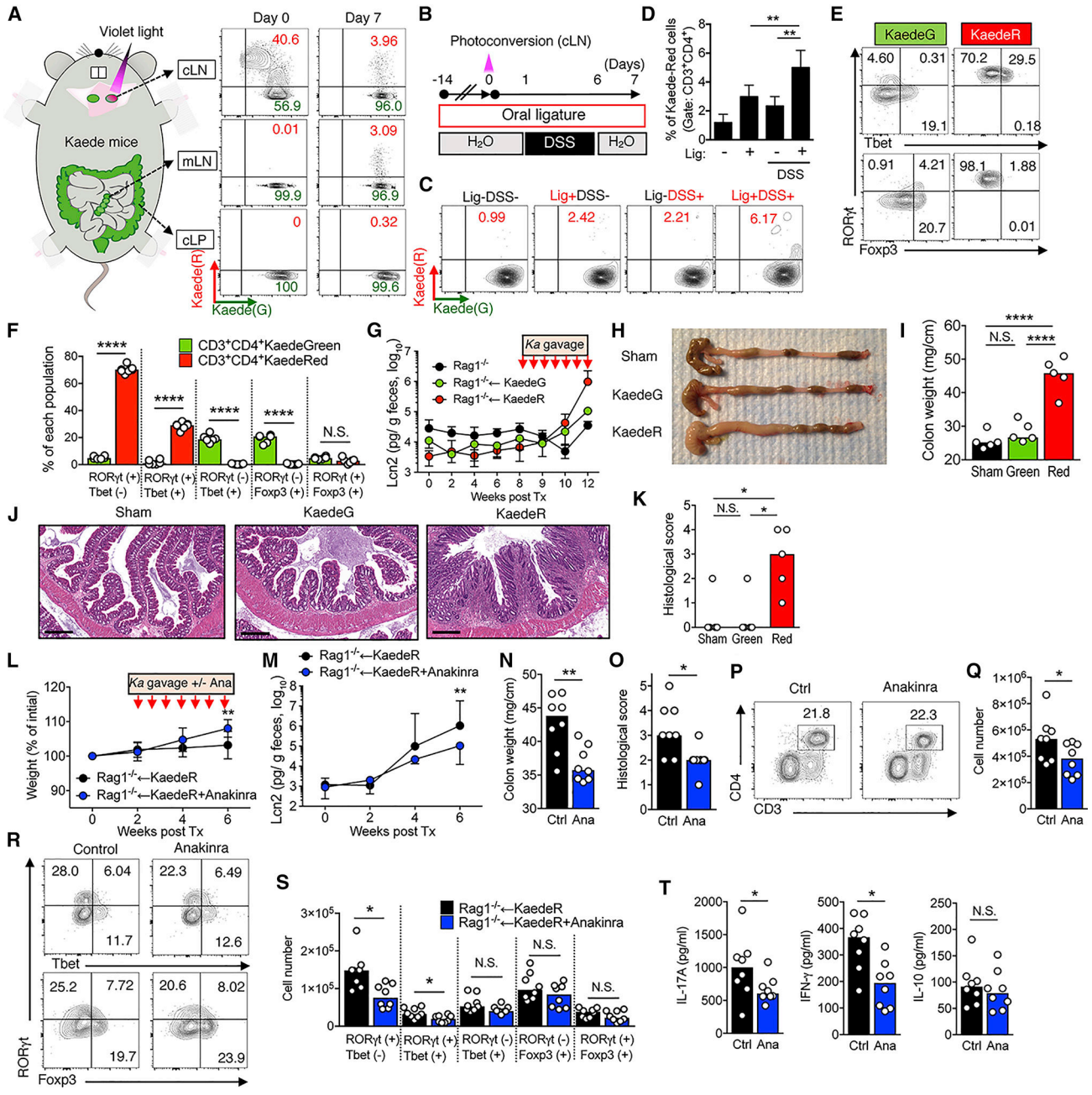

Figure 6. Orally Primed T Cells Migrate to the cLP during Colitis

Cervical LNs of anesthetized Kaede Tg mice were exposed to violet light for 1 min. Mice were then monitored for 7 days. Mononuclear cells were isolated from the cLN, mLN, and colonic LP (cLP) on day 0 (immediately after photoconversion) and day 7. The expression of Kaede-Green and Kaede-Red fluorescence protein in $CD3^+CD4^+$ T cells was analyzed by FACS.

(A) Representative FACS plot data.

(B–D) Oral ligatures were inserted into Kaede Tg mice. Photoconversion of cLNs was performed 14 days after ligature insertion. One day after photoconversion, mice were administered 1.5% DSS for 5 days, followed by water for 1 day. The presence of cLN-

derived $CD4^+$ T cells (Kaede-Red+) in the LP was analyzed by FACS. Representative flow data (C) and quantification (D) are shown.

(E and F) Representative flow cytometry plots and frequencies of Th1, Th17, and Treg cells (gated on Kaede-Green+ or Kaede-Red+ $CD3^+CD4^+$ T cells) in the cLP.

(G) Kaede-Red+ $CD3^+CD4^+$ T cells isolated from ligature–DSS mice or Kaede-Green+ $CD3^+CD4^+$ T cells isolated from DSS mice without ligature were adoptively transferred into SPF *Rag1*$^{-/-}$ mice (2 × 105 cells/mouse, intravenously [i.v.]), respectively. The negative Ctrl group received saline. T cell-transferred *Rag1*$^{-/-}$ mice were then monitored for 8 weeks. 8 weeks after transfer, Ka SK431 (1 × 109 CFUs/mouse) was orally administered 3 times per week for an additional 4 weeks. Also shown are fecal Lcn2 levels at the indicated days after T cell transfer.

(H) Representative images of the colon 12 weeks after transfer.

(I) Colonic weight (milligrams per centimeter).

(J and K) Representative histological images of the colon (scale bar, 300 μm) and histological score of the colon, assessed by the criteria for the T cell transfer colitis model.

(L) Kaede-Red+ $CD3^+CD4^+$ T cells isolated from the colon of ligature-DSS mice were adoptively transferred into SPF *Rag1*$^{-/-}$ mice (as described in G–K). 2 weeks after transfer, Ka SK431 (1 × 109 CFUs/mouse) was administered orally 3 times per week for an additional 4 weeks in the absence or presence of anakinra (50 mg/kg every 2 days, i.p.).

(M) Fecal Lcn2 levels at the indicated days after T cell transfer.

(N) Colon weight (milligrams per centimeter) 6 weeks after transfer.

(O) Histological score of the colon 6 weeks post-transfer, evaluated by the criteria for the T cell transfer colitis model.

(P and Q) Representative flow cytometry plots and numbers of $CD3^+CD4^+$ T cells in the cLP.

(R and S) Representative flow cytometry plots and cell numbers of Th1, Th17, and Treg cells in the cLP.

(T) Cytokine production from $CD4^+$ LP cells re-stimulated with αCD3/28 Abs for 24 h. Results are shown as mean ± SD (two-way ANOVA) or median (one-way ANOVA). Each dot indicates an individual mouse (N = 4–8). *$p < 0.05$, **$p < 0.01$, ****$p < 0.0001$ by Mann-Whitney *U* test (F, N, O, Q, S, and T), one-way ANOVA followed by Bonferroni post hoc test (D, I, and K), or two-way ANOVA followed by Bonferroni post hoc test (L and M).

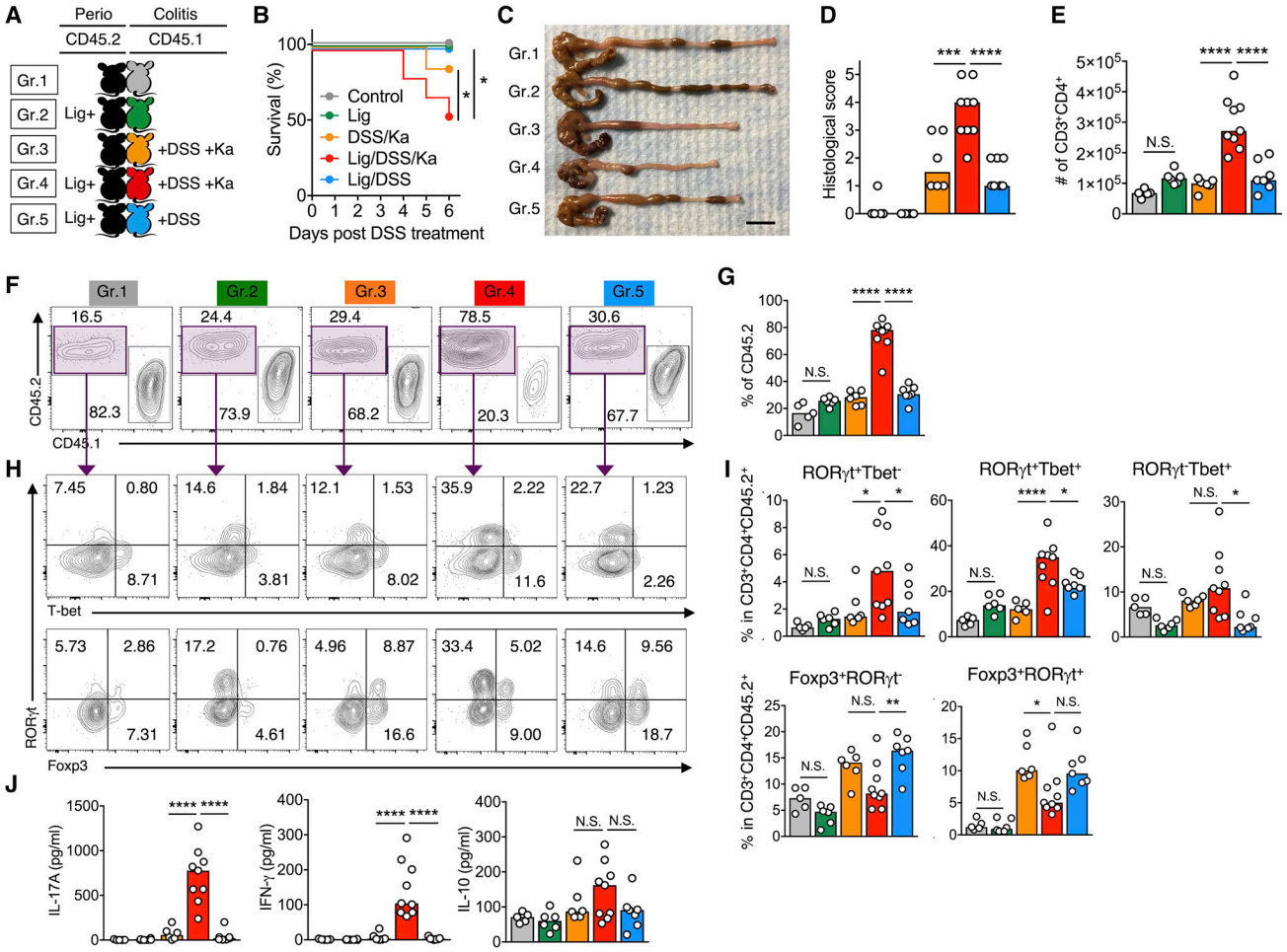

Figure 7. Orally Primed Circulating T Cells Expand in the Gut Colonized by Oral Pathobionts and Aggravate Colitis

(A) Periodontitis was induced in SPF CD45.2 mice (oral ligature [Lig] for 14 days), and then they were surgically connected to SPF CD45.1 congenic mice. After a week, DSS colitis was induced in CD45.1 mice via oral gavage (100 mg/200 μL) daily for 6 days. Ka (109 CFUs) was also supplied to some CD45.1 mice daily for 6 days. On day 6 after DSS/Ka administration, CD45.1 mice were sacrificed and subjected to analyses.

(B) Mortality of CD45.1 mice during the DSS/Ka treatment.

(C) Representative colon images of CD45.1 mice on day 7 after DSS/Ka (scale bar, 1 cm).

(D) Histological score of the colon isolated from CD45.1 mice.

(E) Number of $CD3^+CD4^+$ T cells in cLP isolated from CD45.1 mice.

(F and G) Representative flow cytometry plots and frequencies of CD45.1+ or CD45.2+ (periodontitis mouse-derived) $CD3^+CD4^+$ T cells in the cLP isolated from CD45.1 mice.

(H and I) Representative flow cytometry plots and frequencies of Th1, Th17, and Treg cells in cLP isolated from CD45.1 mice.

(J) Cytokine production from $CD3^+CD4^+$ T cells in cLP isolated from CD45.1 mice. T cells were re-stimulated with αCD3/28 Abs for 24 h.

Results are shown as median (one-way ANOVA). Each dot indicates an individual mouse (N = 5–9). *p < 0.05, **p < 0.01, ***p < 0.001, ****p < 0.0001 by log rank (Mantel-Cox) test (B) or one-way ANOVA followed by Bonferroni post hoc test (D, E, G, I, and J).

KEY RESOURCES TABLE

REAGENT or RESOURCE	SOURCE	IDENTIFIER
Antibodies		
CD45.1 monoclonal Ab (A20), PE-Cy7	Thermo Fisher Scientific	25-0453-82
CD45.2 monoclonal Ab (104), APC-eFluor 780	Thermo Fisher Scientific	47-0454-82
CD3 Monoclonal Ab PerCP-cy5.5 (145-2C11)	Thermo Fisher Scientific	45-0031-82
CD4 Monoclonal Ab (GK1.5), FITC	Thermo Fisher Scientific	11-0041-85
CD44 anti-mouse/human Ab APC/Cy7 (IM7)	Biolegend	103028
CD62 anti-mouse Ab PE/Cy7 (MEL14)	Biolegend	104418
CD25 anti-mouse PE-Cy7 (PC61)	BD	552880
T-bet Monoclonal Ab PE (eBio4B10 (4B10))	Thermo Fisher Scientific	12-5825-80
RORgt anti-mouse Ab BV421 (Q31-378)	Thermo Fisher Scientific	BDB562894
FOXP3 Monoclonal Ab APC (FJK-16 s)	Thermo Fisher Scientific	17-5773-82
CCR9 anti-mouse Ab PE (9B1)	Biolegend	129707
LPAM-1 anti-mouse Ab APC (DATK32)	Biolegend	120607
CD11c anti-mouse Ab PE-Cy7 (N418)	Thermo Fisher Scientific	25-0114-82
CD64 anti-mouse Ab FITC (X54-5/7.1)	Biolegend	139316
CD45 anti-mouse Ab APC-eFluor 780 (30-F11)	Thermo Fisher Scientific	47-0451082
MHC2 Monoclonal Ab eFluor450 (AF6-120.1)	Thermo Fisher Scientific	48-5320-82
Ly6C anti-mouse Ab APC (HK1.4)	Biolegend	128015
IL-1 beta (Pro-form) Monoclonal Ab PE (NJTEN3)	Thermo Fisher Scientific	12-7114-82
CD11c monoclonal antibody (biotinylated)	Thermo Fisher Scientific	13-0114-82
Bacterial and Virus Strains		
Bacterium: *Streptococcus salivarius* SK109	This paper	N/A
Bacterium: *Streptococcus sp. JS71* SK348	This paper	N/A
Bacterium: *Staphylococcus xylosus* SK207	This paper	N/A
Bacterium: *Enterobacter cloacae* SK156	This paper	N/A
Bacterium: *Enterobacter hormaechei* SK232	This paper	N/A
Bacterium: *Klebsiella varicola* SK430	This paper	N/A
Bacterium: *Klebsiella aerogenes* SK431	This paper	N/A
Bacterium: *Klebsiella pneumoniae* SK440	This paper	N/A
Bacterium: *Citrobacter amalonaticus* SK427	This paper	N/A
Bacterium: *Escherichia coli* SK346	This paper	N/A
Bacterium: *Escherichia coli* SK460	This paper	N/A
Bacterium: *Escherichia coli* SK461	This paper	N/A
Bacterium: *Enterococcus faecalis* SK369	This paper	N/A
Bacterium: *Bacteroides thetaiotaomicron* dnLKV9	Bloom et al., 2011	https://pubmed.ncbi.nlm.nih.gov/21575910
Bacterium: *Bacteroides uniformis* dnLKV2	Bloom et al., 2011	https://pubmed.ncbi.nlm.nih.gov/21575910

REAGENT or RESOURCE	SOURCE	IDENTIFIER
Bacterium: Bacteroides *vulgatus* dnLKV7	Bloom et al., 2011	https://pubmed.ncbi.nlm.nih.gov/21575910
Bacterium: *Salmonella enterica* serovar Typhimurium SL1344	Franchi et al., 2012	https://pubmed.ncbi.nlm.nih.gov/22484733
Chemicals, Peptides, and Recombinant Proteins		
Dextran Sodium Sulfate	MP Biomedical	0216011090
Dextran Sodium Sulfate	Cayman	23250
Gentamicin	Thermo Fisher Scientific	15750060
Streptomycin (USP grade)	X-GEN	39822-0706-2
Kineret® (Anakinra, IL-1R antagonist)	Swedish Orphan Biovitrum AB	48899
Recombinant mouse GM-CSF	Biolegend	576304
Human Collagen IV	Sigma	C5533
Collagenase, type3	Worthington	LS004185
DNase I	Worthington	LS006342
RPMI 1640	Thermo Fisher Scientific	21870076
Advanced DMEM/F12	Thermo Fisher Scientific	12634010
HBSS	Thermo Fisher Scientific	14170112
Penicillin-Streptomycin	Thermo Fisher Scientific	15140122
Dithiothreitol	Sigma	D0632
0.5M EDTA (pH 8.0)	Promega	PR-V4231
Percoll	GE Healthcare	17-0891-01
Paraformaldehyde 4%, 1L	Thermo Fisher Scientific	AAJ19943K2
MacConkey agar	SIGMA	M7408
FBS	gibco	16000-044
Cell-ID Cisplatin	Fluidigm	201064
TruStain FcX	Biolegend	101320
Ketalar® (Ketamine)	Par Pharmaceutical, Inc.	42023-115-10
Anased® (Xylazine)	AKORN Animal Health	59399-110-20
RIMADYL® (Carprofen)	Zoetis	RXRIM-INJ
VETONE® (Isoflurane)	Fluriso	13985-528-40
Critical Commercial Assays		
PCR Master Mix	Promega	M7502
E.Z.N.A.Total RNA Kit I	OMEGA	SKU: R6834-01
DNeasy Blood & Tissue Kit	QIAGEN	69506
EasySepTM Mouse $CD4^+$ T Cell Isolation Kit	Thermo Fisher Scientific	NC0471206
EasySep mouse biotin positive selection kit	Thermo Fisher Scientific	NC0845277
eBioscience Foxp3 / Transcription Factor Staining Buffer Set	Thermo Fisher Scientific	00-5523-00
Fixation and Permeabilization Solution	BD	554722
Cell recovery solution	Corning	354253
Golgiplug solution	BDB555029	BDB555029

REAGENT or RESOURCE	SOURCE	IDENTIFIER
High-Capacity RNA-to-cDNA Kit	Thermo Fisher Scientific	4387406
SYBR Green PCR Master Mix	Thermo Fisher Scientific	4309155
Deposited Data		
16S rRNA MiSeq data and bacterial whole genome sequence data	NCBI BioProject	PRJNA631055
Experimental Models: Organisms/Strains, Cell Lines		
Mouse: C57BL/6	The Jackson Laboratory	JAX 000664
Mouse: *Rag1*$^{-/-}$ mice	The Jackson Laboratory	JAX 002216
Mouse: *Il10*$^{-/}$ mice	The Jackson Laboratory	JAX 002251
Mouse: *CD45.1* mice	The Jackson Laboratory	JAX 002014
Mouse: *Il17a-EGFP* mice	The Jackson Laboratory	JAX 018472
Mouse: Kaede mice	The RIKEN BioResource Research Center	RBRC05737
Mouse: *Il1r*$^{-/-}$ mice	The Jackson Laboratory	JAX 003245
Mouse: *Nlrp3*$^{-/-}$ mice	The Jackson Laboratory	JAX 021302
Mouse: *Nlrc4*$^{-/-}$ mice	Franchi et al., 2006	https://pubmed.ncbi.nlm.nih.gov/16648852
Mouse: *Aim2*$^{-/-}$ mice	Seo et al., 2015	https://pubmed.ncbi.nlm.nih.gov/25862092
Mouse: *Nlrp6*$^{-/-}$ mice	Chen et al., 2011	https://www.ncbi.nlm.nih.gov/pmc/articles/PMC3133458/
Mouse: *Pycard*$^{-/-}$ mice	He et al., 2016	https://pubmed.ncbi.nlm.nih.gov/26814970
Mouse: *Casp1*$^{-/-}$ mice	Man et al., 2017	https://pubmed.ncbi.nlm.nih.gov/28345580
Mouse: *Casp11*$^{-/-}$ mice	He et al., 2016	https://pubmed.ncbi.nlm.nih.gov/26814970
Mouse: *Myd88*$^{-/-}$ mice	Adachi et al., 1998	https://pubmed.ncbi.nlm.nih.gov/9697844
Mouse: Germ-free C57BL/6	Germ-free Facility at University of Michigan	N/A
Mouse: Germ-free C57BL/6	National Gnotobiotic Rodent Resource Center	N/A
Mouse: Germ-free C57BL/6 *Il10*$^{-/-}$	Germ-free Facility at University of Michigan	N/A
Mouse: Germ-free C57BL/6 *Il10*$^{-/-}$	National Gnotobiotic Rodent Resource Center	N/A
Mouse: Germ-free *Rag1*$^{/-}$	Germ-free Facility at University of Michigan	N/A
T84 human colorectal cancer cell line	ATCC	ATCC CCL-248
Oligonucleotides		
See Table S3 for primers	N/A	N/A
Software and Algorithms		
Mothur v1.39.0	Schloss et al., 2009	N/A
Prism v7.0c	GraphPad Software	https://www.graphpad.com/scientific-software/prism/

REAGENT or RESOURCE	SOURCE	IDENTIFIER
Flowjo v10.0.7	BD	https://www.flowjo.com/
CytoBank v7.3.0	CytoBank	https://support.cytobank.org/hc/en-us/articles/204369428-Introduction-to-viSNE-in-Cytobank-
Microview v2.5.0	Parallax innovations	http://www.parallax-innovations.com/microview.html
SPAdes v 3.13.0	Bankevich et al., 2012	http://cab.spbu.ru/software/spades/
Other		
Anaerobic chamber	Coy manufacturing	Vinyl Type A + Type B
Mini-BeadBeater-16	Thermo Fisher Scientific	NC0342321
Garnet beads, 0.7mm	QIAGEN	13123-50
Collimated Diode Laser System	Laserglow Technologies	LRD-0405
CyTOF Helios system	Fluidigm	N/A
Illumina MiSeq (500v2) platform	Illumina	N/A
FACSAria II	BD	N/A
LSRFortessa	BD	N/A
FACSCelesta	BD	N/A
BD Autoclip Wound Closing System	Thermo Fisher Scientific	22-275998
Wound Clip (Case of 10 PK)	Thermo Fisher Scientific	01-804-5
Roboz Surgical 5-0 SUTURE BLACK SILK	Thermo Fisher Scientific	NC9422522
Ethilon Suture 5-0 Nylon P-3 Undyed 18” Monofilament	Ethicon	6544169
Veet (Depilatory cream)	Reckitt Benckiser Parsippany (Walmart)	46280011302